BIOCHEMISTRY
including biophysical chemistry & molecular biology

Article

pubs.acs.org/biochemistry

Concurrent Increases and Decreases in Local Stability and Conformational Heterogeneity in Cu, Zn Superoxide Dismutase Variants Revealed by Temperature-Dependence of Amide Chemical Shifts

Colleen M. Doyle,[†] Jessica A. Rumfeldt,[†] Helen R. Broom,[†] Ashok Sekhar,[‡,§,∥] Lewis E. Kay,[‡,§,∥,⊥] and Elizabeth M. Meiering*[,†]

[†]Department of Chemistry, University of Waterloo, Waterloo, Canada

[‡]Department of Molecular Genetics, [§]Department of Biochemistry, [∥]Department of Chemistry, University of Toronto, Toronto, Canada

[⊥]Program in Molecular Structure and Function, Hospital for Sick Children, Toronto, Canada

Supporting Information

ABSTRACT: The chemical shifts of backbone amide protons in proteins are sensitive reporters of local structural stability and conformational heterogeneity, which can be determined from their readily measured linear and nonlinear temperature-dependences, respectively. Here we report analyses of amide proton temperature-dependences for native dimeric Cu, Zn superoxide dismutase (holo pWT SOD1) and structurally diverse mutant SOD1s associated with amyotrophic lateral sclerosis (ALS). Holo pWT SOD1 loses structure with temperature first at its periphery and, while having extremely high global stability, nevertheless exhibits extensive conformational heterogeneity, with ∼1 in 5 residues showing evidence for population of low energy alternative states. The holo G93A and E100G ALS mutants have moderately decreased global stability, whereas V148I is slightly stabilized. Comparison of the holo mutants as well as the marginally stable immature monomeric unmetalated and disulfide-reduced (apo^{2SH}) pWT with holo pWT shows that changes in the local structural stability of individual amides vary greatly, with average changes corresponding to differences in global protein stability measured by differential scanning calorimetry. Mutants also exhibit altered conformational heterogeneity compared to pWT. Strikingly, substantial increases as well as decreases in local stability and conformational heterogeneity occur, in particular upon maturation and for G93A. Thus, the temperature-dependence of amide shifts for SOD1 variants is a rich source of information on the location and extent of perturbation of structure upon covalent changes and ligand binding. The implications for potential mechanisms of toxic misfolding of SOD1 in disease and for general aspects of protein energetics, including entropy−enthalpy compensation, are discussed.

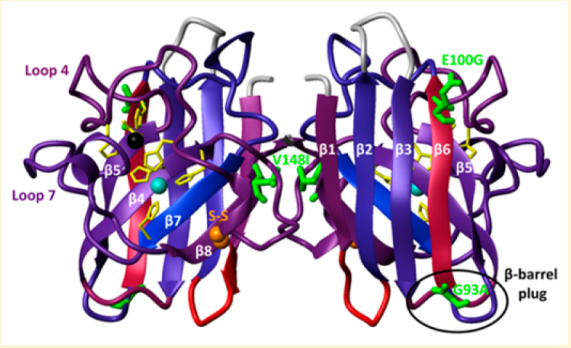

The native states of proteins are well established as consisting of an ensemble of interconverting conformations. The dynamics of these conformations are central to protein stability, binding, allostery, and catalysis in ways that remain difficult to explain and predict.[1−4] Protein dynamics are challenging to characterize as they are invisible to many standard techniques and occur on many different time scales with varying energetics. Measurement of the temperature-dependence of chemical shifts by nuclear magnetic resonance (NMR) is a powerful approach that can provide high resolution information on both local structure and conformational heterogeneity in proteins.[5−23] In particular, the linear dependence of amide proton chemical shifts (δ_{NH}) on temperature, known as the temperature coefficient, $\Delta\delta_{NH}/\Delta T$, is well established as being sensitive to hydrogen bond formation.[5,7,12,13,23,24] However, recent work has found that a larger determinant of $\Delta\delta_{NH}/\Delta T$ is the temperature-dependent loss of structure[18] and that the average and spread of $\Delta\delta_{NH}/\Delta T$ values reports on structure even in the absence of persistent intramolecular hydrogen bonding.[8,25] Here, we explore further how $\Delta\delta_{NH}/\Delta T$ can be used to characterize temperature-dependent loss of structure within proteins, which we refer to as "structural stability."

In addition, the *nonlinearity* of the temperature-dependence of δ_{NH} can report on the population of alternative states of proteins, i.e., "conformational heterogeneity."[6] Previous studies of various proteins have found that between 5% and 40% of amide protons

Received: October 16, 2015
Revised: February 2, 2016
Published: February 5, 2016

DOI: 10.1021/acs.biochem.5b01133
Biochemistry 2016, 55, 1346−1361

exhibit curved temperature-dependences.[6,7,10,17,19,20] The curvature was modeled in terms of the population of an alternative state in fast exchange on the chemical shift time scale with the ground state and within ~5 kcal/mol in energy.[6,20] Thus, measurements of curvature can report on alternative states close in energy to the native state and may complement other NMR methods for identifying and structurally characterizing thermally accessible low lying biomolecular conformations.[26−32] To date, comparisons of the temperature-dependences of δ_{NH} for related proteins have been limited, for example, to characterizing similarities and differences between homologous proteins from different organisms or caused by myristoylation.[10,19]

Here, we apply measurements of $\Delta\delta_{NH}/\Delta T$, as well as nitrogen chemical shift temperature-dependence ($\Delta\delta_N/\Delta T$) which have been less studied, and curvature of δ_{NH} to investigate changes caused by maturation and disease-associated mutations for human Cu, Zn superoxide dismutase (SOD1). This homodimeric metalloenzyme consists of 153 amino acid subunits, each binding 1 Cu^{2+} and 1 Zn^{2+}, containing a conserved intrasubunit disulfide bond and adopting an immunoglobulin-like antiparallel β-barrel fold with an N-terminal sheet (strands 1, 2, 3, and 6) and a C-terminal sheet (strands 4, 5, 7, and 8).[33] The fully mature (holo) protein is highly structured and extremely stable ($\Delta G \approx 33$ kcal (mol dimer)$^{-1}$ at 37 °C).[34−36] In contrast, the most immature form of SOD1, lacking bound metals and with reduced disulfide bond (apo^{2SH}), adopts a highly dynamic, monomeric structure[16] that is marginally stable ($\Delta G = 1.8$ kcal (mol monomer)$^{-1}$ at 37 °C).[37] To date, over 170 mutations in SOD1, which span the entire polypeptide chain, have been associated with causing the devastating neurodegenerative disease amyotrophic lateral sclerosis (ALS) (http://alsod.iop.kcl.ac.uk/).[38] A hallmark feature of ALS is the appearance of protein aggregates in motor neurons. Extensive evidence supports the hypothesis that mutant SOD1s cause disease by undergoing toxic misfolding and aggregation; however, the underlying mechanisms remain unclear.[39−41]

We find that analyses of temperature-dependence for δ_{NH} are a rich source of information on the changes in structural stability and conformational heterogeneity that occur in SOD1 upon maturation and mutation. The results for holo pseudo wild-type (pWT; see Experimental Procedures) are consistent with its high global stability, but also highlight less stable regions in the protein and extensive evidence for sampling of alternative states, mainly for residues at the periphery of the structure. Comparison of holo with apo^{2SH} shows that the immature monomer, while being much more dynamic, nevertheless has a well formed β-barrel with some regions, surprisingly, more structured locally than in the mature dimer. The holo form is also characterized for structurally diverse ALS-associated mutants: G93A, in a tight turn; E100G, in a β-strand; and V148I, in the dimer interface, providing the first detailed stability analyses for E100G and V148I. The mutants exhibit common features but also distinctive changes in structural stability and conformational heterogeneity. These high resolution analyses of SOD1 give insights into the molecular mechanisms by which local changes due to maturation or mutation can be transmitted through the protein and impact global stability, as well as modes of aggregation that may occur in disease.

EXPERIMENTAL PROCEDURES

Preparation and Purification of Recombinant SOD1. All SOD1 variants studied are in the pseudo wild-type (pWT) background, where the free cysteines at positions 6 and 111 have been replaced by alanine and serine, respectively. The structure, activity, and stability of pWT are very similar to wild-type SOD1.[34,42−44] Recombinant pWT and mutant SOD1 were expressed as previously described[45,46] and purified using a modification of the procedure of Getzoff et al. in which a Poros HP2 hydrophobic interaction column replaced the diethylaminoethyl column.[45] ^{15}N-Labeled SOD1 was prepared by growing *Escherichia coli* in M9 minimal media with $^{15}NH_4Cl$ as the sole nitrogen source.

NMR Sample Preparation. Purified ^{15}N-labeled pWT and mutant SOD1 was exchanged into buffer (20 mM hydroxyethyl piperazine *N*′-2-ethanesulfonic acid (HEPES), pH 7.8) by ultrafiltration (Ultracel 3K, Millipore) to a final concentration of ~30 mg/mL. The copper was reduced to Cu^{1+} by addition of 5 mM sodium isoascorbate to avoid paramagnetic line broadening by Cu^{2+}.

NMR Spectroscopy. ^{1}H−^{15}N HSQC spectra were acquired at temperatures ranging from 297 K (24 °C) to 348 K (75 °C). For each variant the NMR thermal titration was completed in duplicate, using ~5 and 10 °C increments. The final set of temperature coefficients for each variant is the average of the two independent experiments. All NMR experiments were performed on a Bruker Avance 600 MHz spectrometer, with the exception of V148I for which one temperature-dependence experiment was completed on a Bruker Avance 500 MHz spectrometer. Proton chemical shifts were referenced to internal water. A correction for the temperature-dependence of water was applied.[47] Temperature was confirmed using the chemical shift separation of water referenced to 4,4-dimethyl-4-silapentane-1-sulfonic acid, as water has a known linear temperature-dependence,[47] and using a thermocouple. NMR data were processed using the Bruker XWIN-NMR 3.5 software and analyzed using computer aided resonance assignment (CARA).[48] Sequence specific resonance assignments were determined previously for pWT SOD1 and the mutants G93A and E100G at 25 °C, pH 7.8.[49] Resonance assignments for V148I were made using a ^{15}N-edited NOESY-HSQC experiment at 24 °C, pH 7.8. NOE cross peaks were used to assign the peaks that shifted upon mutation and confirm the assignment of those that did not.

Amide Chemical Shift versus Temperature Calculations. For each residue, the δ_{NH} and δ_N were plotted as a function of temperature (in K) and fit to a straight line by linear regression. The slope of this line represents the temperature coefficient ($\Delta\delta/\Delta T$).[7] Experimental uncertainties in $\Delta\delta_{NH}/\Delta T$ were determined using a δ_{NH} uncertainty of 0.005 ppm. The ^{1}H−^{15}N HSQC crosspeaks for ~20 amides in the holo SOD1 variants lose intensity and are no longer observable at increased temperatures; for consistency, temperature coefficients were calculated and compared only for residues with observable signals over the full temperature range (~24−75 °C). Deviations from linearity (residuals) were calculated by subtracting the observed chemical shifts from the straight line.[6] Residuals (y) were plotted versus temperature (x) and fit to a quadratic equation ($y = ax^2 + bx + c$). The quadratic coefficient, a, provides a measure of the magnitude of curvature. All protons for which the quadratic coefficient differed from zero at $p < 0.01$ (using a δ_{NH} uncertainty of 0.005 ppm) were considered to have curved temperature-dependences.

Differential Scanning Calorimetry (DSC). DSC experiments were performed as described[36] using a MicroCal LLC VP-DSC (MicroCal Inc., Northampton, MA). All samples contained 0.2 to ~2 mg mL^{-1} holo SOD1 in 20 mM HEPES, pH 7.8. The

DOI: 10.1021/acs.biochem.5b01133
Biochemistry 2016, 55, 1346−1361

scan rate was 1 °C min^{-1}. DSC data were fit to a two-state transition between folded dimer and unfolded monomers, $N_2 \leftrightarrow 2U$, as described previously.[36,50,51]

RESULTS

Differential Scanning Calorimetry shows Global Stability Is Moderately Decreased for Holo G93A and E100G and Slightly Increased for Holo V148I. The global stability of all the SOD1s studied here was measured by DSC for comparison with NMR data. The temperature where half of the protein is unfolded (T_m), the van't Hoff enthalpy of unfolding (ΔH_{vH}) and the ratio of ΔH_{vH} and the calorimetric enthalpy of unfolding (ΔH_{cal}) are given in Table 1. Since the T_m for a dimer is concentration dependent,[51] the T_m's were also calculated for 30 mg mL^{-1} protein (the approximate concentration of an NMR sample; Table 2) using the parameters obtained for the DSC measurements at lower protein concentration (Table 1; Figure S1). Relative to pWT, the melting temperatures (T_m's) for holo E100G and G93A are decreased by ~4−5 °C but increased by ~1 °C for V148I and remain >91 °C for all variants (Table 2). In contrast, apo^{2SH} pWT has a much lower T_m of 47.6 °C.[37] Chemical shifts were measured for ~24−75 °C for holo variants and previously for 10−30 °C for reduced apo;[16] the highest temperatures are well below the global unfolding transitions for the proteins (Figure S1).[7,36,37] Thus, changes in chemical shift with temperature are determined by local rather than global unfolding.

Table 1. DSC Fitted Parameters for SOD1s

SOD1[a]	[protein] (mg mL^{-1})	T_m (°C)	ΔH_{vH} (kcal mol^{-1})	$\Delta H_{vH}/\Delta H_{cal}$
holo pWT[b]	6.30	94.2 ± 0.3	238.7 ± 20.2	0.85
holo pWT[b]	1.87	93.2 ± 0.3	276.9 ± 20.5	1.02
holo pWT[b]	1.00	92.5 ± 0.5	269.0 ± 30.5	1.05
holo pWT[b]	1.00	93.2 ± 0.0	272.6 ± 4.0	0.90
holo pWT[b]	1.00	93.1 ± 0.2	268.8 ± 10.6	1.01
holo pWT[b]	0.50	91.6 ± 0.5	230.6 ± 24.3	1.04
holo pWT[b]	0.50	92.4 ± 0.4	256.5 ± 22.8	1.10
holo pWT[b]	0.20	91.6 ± 0.2	265.5 ± 15.1	1.15
mean ± SD[d]				1.02 ± 0.10
apo^{2SH} pWT[c]	2.30	47.2 ± 0.1	59.8 ± 1.7	1.34
apo^{2SH} pWT[c]	0.93	47.7 ± 0.3	62.7 ± 3.2	1.22
apo^{2SH} pWT[c]	0.55	48.8 ± 0.0	60.6 ± 0.7	1.01
apo^{2SH} pWT[c]	0.53	47.5 ± 0.0	60.2 ± 0.6	1.00
apo^{2SH} pWT[c]	0.48	47.8 ± 0.6	62.5 ± 5.4	1.05
apo^{2SH} pWT[c]	0.42	47.4 ± 0.3	63.2 ± 2.8	1.21
apo^{2SH} pWT[c]	0.25	47.0 ± 0.5	60.4 ± 1.1	0.96
apo^{2SH} pWT[c]	0.11	47.3 ± 0.1	63.5 ± 1.7	1.33
mean ± SD[d]				1.14 ± 0.15
holo G93A[b]	1.00	88.5 ± 0.0	244.9 ± 8.0	1.22
holo G93A[b]	1.00	88.4 ± 0.3	234.6 ± 12.0	1.04
holo G93A[b]	0.50	87.4 ± 0.1	194.3 ± 4.5	0.87
holo G93A[b]	0.20	86.6 ± 0.4	207.8 ± 17.7	0.90
mean ± SD[d]				1.01 ± 0.16
holo E100G	2.00	88.2 ± 0.3	255.2 ± 27.9	0.87
holo E100G	1.00	86.9 ± 0.1	227.4 ± 55.8	0.86
holo E100G	0.50	86.5 ± 0.2	224.2 ± 25.3	0.83
holo E100G	0.20	85.4 ± 0.1	210.5 ± 43.9	0.85
mean ± SD[d]				0.85 ± 0.02
holo V148I	2.11	93.2 ± 0.0	262.0 ± 2.4	0.78
holo V148I	1.00	92.5 ± 0.0	254.5 ± 1.8	0.77
holo V148I	0.51	91.9 ± 0.0	251.6 ± 2.8	0.81
holo V148I	0.19	92.1 ± 0.1	216.4 ± 4.5	0.62
Mean ± SD[d]				0.75 ± 0.09

[a]Data for holo SOD1s were fit as described previously[36] to a dimer two-state model. [b]Values for holo pWT and G93A are from ref 36. [c]Values for apo^{2SH} pWT are from fits to a monomer 2-state model.[37] Error estimates for fitted T_m values are from the fitting program (Origin 5.0) and error estimates for ΔH_{vH} are propagated according to standard procedures[99] from fitted errors in Δh, the specific enthalpy of unfolding, and β, $\Delta H_{vH}/\Delta H_{cal}$ × molecular weight of the SOD1 homodimer.[36] [d]SD, standard deviation.

Temperature Coefficients of Holo pWT SOD1 Indicate High Global Protein Stability, and Disruption of Structure with Temperature First at its Less Stable Periphery. For holo pWT SOD1, the average of all measured $\Delta\delta_{NH}/\Delta T$ is −3.2 ppb/K (Table 2), which is a notably low (less negative) value compared to other proteins.[5] On the other hand, the range of temperature coefficients is comparable to those of other stable globular proteins (typically, ~ −11 to 1 ppb/K).[12] The low average value for holo pWT is consistent with the presence of extensive intramolecular hydrogen bonds throughout the protein, which are generally associated with $\Delta\delta_{NH}/\Delta T$ values less negative than −4.6 ppb/K.[12,13] The results are therefore in agreement with X-ray crystallography and NMR structural data, as well as thermodynamic data, indicating holo SOD1 is highly structured and stable.[16,34−36,44,52]

Clear differences in local structural stability are apparent from the analysis of $\Delta\delta_{NH}/\Delta T$. The average δ_{NH} temperature coefficients for secondary structural elements ($\Delta\delta_{NH}/\Delta T_{avg}$; Table 2) show that the N-terminal β-sheet is more flexible than the C-terminal β-sheet, with $\Delta\delta_{NH}/\Delta T_{avg}$ values of −3.4 ppb/K and −2.8 ppb/K, respectively. Previous studies of rapid (ps−ns) backbone dynamics by ^{15}N-relaxation measurements[52] and estimates by RCI[16,53] at 25 °C, as well as molecular dynamics simulations,[54] found that all 8 β-strands in holo pWT exhibit comparable, very limited dynamics. In contrast, $\Delta\delta_{NH}/\Delta T$ measurements reveal marked differences in local structural stability (Figure 1). Among the β-barrel strands, β6 has the highest propensity to become disordered with temperature, with a $\Delta\delta_{NH}/\Delta T_{avg}$ of −4.7 ppb/K, followed by β1 and β8 (Table 2). All three are edge strands in the structure (Figure 1), highlighting an inherently lower structural stability in these regions. The β7 strand appears most structured, with $\Delta\delta_{NH}/\Delta T_{avg}$ of −1.8 ppb/K; it is located in the center of the protein protected by the long loops 4 and 7. We note that these long loops, although lacking data for some amide protons, have similar $\Delta\delta_{NH}/\Delta T_{avg}$ values to the β-strands (Table 2), indicating they are highly structured in the holo state.

At an individual residue level, $\Delta\delta_{NH}/\Delta T$ values reveal regions of lower stability at the edge of the structure and higher stability in the core (Figure 1B). Less structured residues with large negative $\Delta\delta_{NH}/\Delta T$ values (<−5.5 ppb/K) tend to occur at the ends of β-strands, in loops, near the dimer interface and in the edge strands, β5 (C-terminal portion) and β6. More structured residues ($\Delta\delta_{NH}/\Delta T$ > −2.5 ppb/K) are concentrated in the core of the protein. When comparing $\Delta\delta_{NH}/\Delta T$ values to amide exchange rates for holo pWT measured under the same buffer and pH conditions,[49] no significant correlation is apparent for SOD1. This may be expected as amide exchange rates are strongly influenced by intramolecular hydrogen bonding and surface exposure, factors which have less of an impact on $\Delta\delta_{NH}/\Delta T$ values.[5,18]

Temperature Coefficients Reveal Large Changes, Including Unexpected Increases as well as Extensive

DOI: 10.1021/acs.biochem.5b01133
Biochemistry 2016, 55, 1346−1361

Table 2. Amide Proton Temperature Coefficient ($\Delta\delta_{NH}/\Delta T$) and Global Stability Data for SOD1 Variants

	$\Delta\delta_{NH}/\Delta T$ (ppb/K)				
overall	holo pWT	apo^{2SH} pWT	holo G93A	holo E100G	holo V148I
average[a]	−3.24 (95)	−4.61 (117)	−3.43 (101)	−3.37 (93)	−3.02 (92)
standard deviation	2.16	3.05	2.48	2.31	2.03
average $\Delta\Delta\delta_{NH}/\Delta T$[a,b]	n/a	0.82 (78)	0.09 (87)	0.16 (83)	−0.14 (81)
minimum	−11.7	−21.5	−14.0	−12.0	−9.0
Average δ_{NH} Temperature Coefficient ($\Delta\delta_{NH}/\Delta T_{avg}$) by Structural Feature (ppb/K)[a]					
N-terminal β-sheet	−3.44 (26)	−3.54 (30)	−3.28 (23)	−3.3 (20)	−3.34 (22)
C-terminal β-sheet	−2.83 (26)	−4.18 (25)	−2.98 (26)	−2.96 (27)	−2.66 (22)
β1	−3.66 (6)	−4.57 (6)	−4.03 (4)	−3.92 (4)	−4.48 (3)
loop 1	−5.47 (2)	−5.48 (4)	na	na	na
β2	−2.64 (6)	−2.42 (8)	−2.13 (7)	−2.52 (6)	−1.97 (6)
loop 2	na	−4.85 (4)	na	na	na
β3	−2.76 (7)	−2.24 (8)	−2.93 (5)	−2.81 (6)	−2.46 (6)
loop 3	−4.02 (2)	−10.39 (3)	−10.07 (2)	−4.22 (2)	−3.98 (2)
β4	−3.08 (7)	−5.54 (7)	−2.91 (8)	−2.95 (8)	−2.57 (6)
loop 4 (50−62)	−3.27 (7)	−5.74 (10)	−3.37 (8)	−3.77 (6)	−2.05 (8)
loop 4 (63−82)	−3.66 (11)	−5.54 (4)	−4.08 (12)	−4.24 (12)	−3.99 (13)
β5	−3.05 (7)	−4.85 (4)	−3.47 (6)	−3.54 (6)	−3.29 (6)
loop 5	−2.76 (3)	−3.17 (4)	−4.24 (4)	−2.77 (3)	−3.15 (4)
β6	−4.69 (7)	−4.95 (8)	−4.05 (7)	−3.96 (4)	−4.47 (7)
loop 6	−2.61 (7)	−4.36 (12)	−2.61 (7)	−2.86 (7)	−2.7 (8)
β7	−1.78 (5)	−3.18 (5)	−1.95 (4)	−1.9 (6)	−1.71 (5)
loop 7	−3.09 (11)	−5.57 (19)	−2.79 (15)	−2.7 (11)	−2.14 (9)
β8	−3.39 (7)	−3.13 (9)	−3.61 (8)	−3.46 (7)	−3.08 (5)
Global Stability					
T_m (°C)[c]	96.3	47.6[d]	92.5	91.1	97.0
ΔT_m (°C)	n/a	−48.7	−3.8	−5.2	+0.7
maximum	1.7	5.4	1.7	1.6	1.9

[a]The number of residues included in each average is given in brackets. Average values for structural features for which there is data for ≤1 residue are indicated by na (not applicable). The number of amides analyzed for holo variants is lower than for apo^{2SH} pWT due to loss of signals at the much higher temperatures used (24−75 °C for holo versus 10−30 °C for apo^{2SH}; see Experimental Procedures). [b]$\Delta\Delta\delta_{NH}/\Delta T$ values are calculated by subtracting $\Delta\delta_{NH}/\Delta T$ for apo^{2SH} pWT or mutant SOD1 from $\Delta\delta_{NH}/\Delta T$ for holo pWT and therefore includes only residues for which direct comparisons to holo pWT can be made. [c]T_m (temperature where half of the protein is unfolded) was calculated from fitted DSC parameters for a protein concentration of NMR samples of 30 mg mL^{-1} (Table 1, Figure S1). [d]T_m for apo^{2SH} pWT is the average value measured for 0.1−2.3 mg/mL protein.[100] Since apo^{2SH} is monomeric the T_m does not vary with protein concentration.[51]

Decreases, in Local Structural Stability for apo^{2SH} Compared to Holo pWT SOD1. We compared $\Delta\delta_{NH}/\Delta T$ for dimeric holo pWT to monomeric apo^{2SH} pWT to assess changes in structural stability associated with maturation, i.e., due to subunit association, metal binding, and disulfide bond formation. The average $\Delta\delta_{NH}/\Delta T$ for the marginally stable pWT apo^{2SH} is −4.6 ppb/K,[16] considerably more negative than the value of −3.2 ppb/K for the much more stable holo protein (Table 2). Also, the range of $\Delta\delta_{NH}/\Delta T$ for apo^{2SH} is markedly greater than for holo, spanning 26.9 ppb/K versus 13.4 ppb/K, respectively (Table 2). Thus, the average $\Delta\delta_{NH}/\Delta T$ values are consistent with the global protein stability.

At the level of local stability for secondary structural elements (Table 2) and individual residues (Figure 2), $\Delta\delta_{NH}/\Delta T$ values reveal wide-ranging differences between holo and apo^{2SH}. The $\Delta\delta_{NH}/\Delta T_{avg}$ values indicate a similar extent of structuring for the N-terminal β-sheet in both holo and apo^{2SH} (−3.4 ppb/K and −3.5 ppb/K, respectively; Table 2). The C-terminal β-sheet, on the other hand, has markedly higher propensity to become disordered in apo^{2SH} compared to holo (−2.8 ppb/K and −4.2 ppb/K, respectively). Considering that the C-terminal β-sheet contains four out of the seven metal binding residues and the disulfide bond (Figure 1A), it is structurally reasonable that this sheet is more disordered in immature SOD1.

Analysis of $\Delta\delta_{NH}/\Delta T_{avg}$ by secondary structural elements (Table 2) reveals that in apo^{2SH}, β-strands 4 and 7 show decreased structural stability. There are two residues that exhibit particularly high disorder in these strands, F45 (β4) and H120 (β7), which lie very close to or participate in the Cu-binding site, respectively. In contrast to holo pWT, in apo^{2SH} pWT the long active site loops, 4 and 7, have $\Delta\delta_{NH}/\Delta T_{avg}$ values more negative than the least stable β-strand (Table 2). It should be noted, though, that there are few resonance assignments in apo^{2SH} pWT for loop 4 surrounding the Zn^{2+}-binding site, due to disorder in this region.[16]

Unexpectedly, residue-specific changes in $\Delta\delta_{NH}/\Delta T$ for apo^{2SH} pWT relative to holo pWT reveal widespread *increases* in structuring as well as decreases (Figure 2). For comparison purposes, we focus on the 41 residues with differences from pWT in $\Delta\delta_{NH}/\Delta T$ ($\Delta\Delta\delta_{NH}/\Delta T$) greater than ±1 ppb/K. As may be expected, the largest decreases in structuring in apo^{2SH} (red and orange in Figure 2) are observed closest to the sites of maturation, i.e., near the metal binding sites and disulfide bond, including in β4, the active site loops (4 and 7) and β8. Surprisingly, moving away from these regions toward the periphery of the structure, the protein tends to become *more* structured (blue and navy in Figure 2), i.e., in β6. Further, some residues in the dimer interface region (G114, T116, A145, and

DOI: 10.1021/acs.biochem.5b01133
Biochemistry 2016, 55, 1346−1361

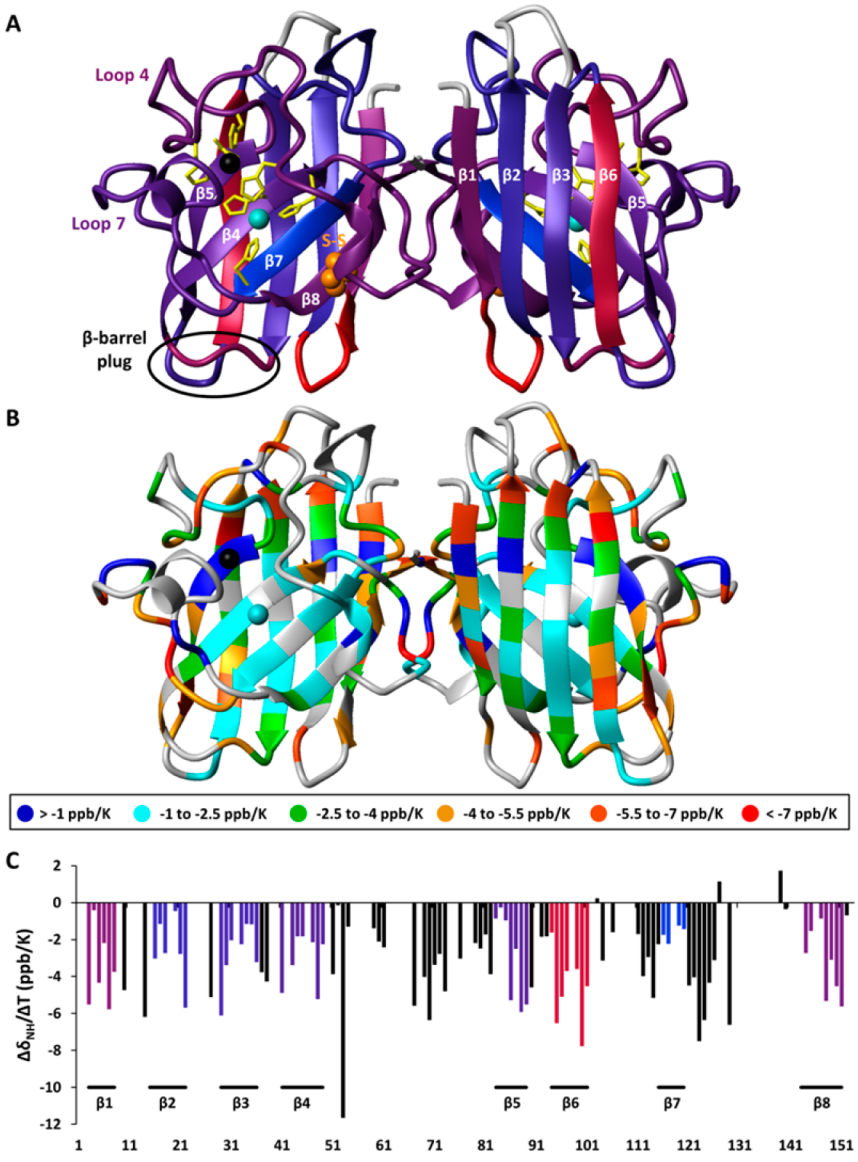

Figure 1. Amide proton temperature coefficients ($\Delta\delta_{NH}/\Delta T$) for holo pWT SOD1 at pH 7.8. (A) $\Delta\delta_{NH}/\Delta T$ averaged by secondary structural elements (Table 2; $\Delta\delta_{NH}/\Delta T_{avg}$) and mapped onto the 3D ribbon structure of holo pWT (PDB 1SOS).[44] Bound Cu (turquoise) and Zn (black) are shown as spheres. Side chains of metal binding ligands (H46, H48, H63, and H120 for Cu, and H63, H71, H80, D83 for Zn) are shown in stick representation, colored yellow. Cys57 and Cys 146, which form the intramolecular disulfide bond, are shown in orange space-filling representation. Structural elements are colored by a red to blue gradient, with red representing the least stable structural element (loop 1) and blue the most stable (β7). Gray represents regions for which there is only one data point and an average could not be calculated. (B) $\Delta\delta_{NH}/\Delta T$ for individual residues mapped onto the 3D ribbon structure of holo pWT. The color scheme is given in the legend. Gray indicates residues for which no data are available. Ribbon diagrams were generated using MOLMOL[101] and PDB file 1SOS.[44] (C) Bar chart of $\Delta\delta_{NH}/\Delta T$. Horizontal bars indicate β-strands. Vertical bars in β-strands are colored according to the color scheme in panel A.

G150) are *more* structured in monomeric apo^{2SH} than in holo. These changes suggest the β-barrel is well folded in monomeric apo^{2SH} SOD1; such structure may be critical to protect against aggregation. The results suggest that maturation to the holo dimer creates strain in the interface which propagates to the periphery of the structure; this may be significant for understanding propagating effects of mutations in holo SOD1, considered below.

Temperature Coefficients Reveal Mutations Cause Changes in Structure that Correlate with Global Stability via Distinct Local and Propagating Effects. The effects of G93A, E100G, and V148I on the structure of holo SOD1 were analyzed using changes in backbone chemical shifts (calculated as the weighted average difference in δ_{NH} and δ_N between mutant and pWT, $\Delta\delta^{15}N^1H$; Figure 3) and $\Delta\delta_{NH}/\Delta T$ (Table 2, Figure 4). Remarkably, these two measures give very similar indications of the regions where perturbations occur upon mutation. Overall, the changes in backbone chemical shifts and $\Delta\delta_{NH}/\Delta T$ are moderate in magnitude, with residues exhibiting the largest changes clustered near the sites of the mutations and smaller changes propagating through the structure (Figures 3 and 4).

Notably, the average $\Delta\Delta\delta_{NH}/\Delta T$ values roughly match the changes in global stability for all the SOD1 variants studied (Table 2). For reference, a positive $\Delta\Delta\delta_{NH}/\Delta T$ indicates a larger (more negative) $\Delta\delta_{NH}/\Delta T$ for the mutant relative to pWT indicating reduced structural stability, and vice versa (Figure 4). Thus, V148I, which has the highest T_m, has a relatively small negative average $\Delta\Delta\delta_{NH}/\Delta T$ value, while the destabilized

DOI: 10.1021/acs.biochem.5b01133
Biochemistry 2016, 55, 1346−1361

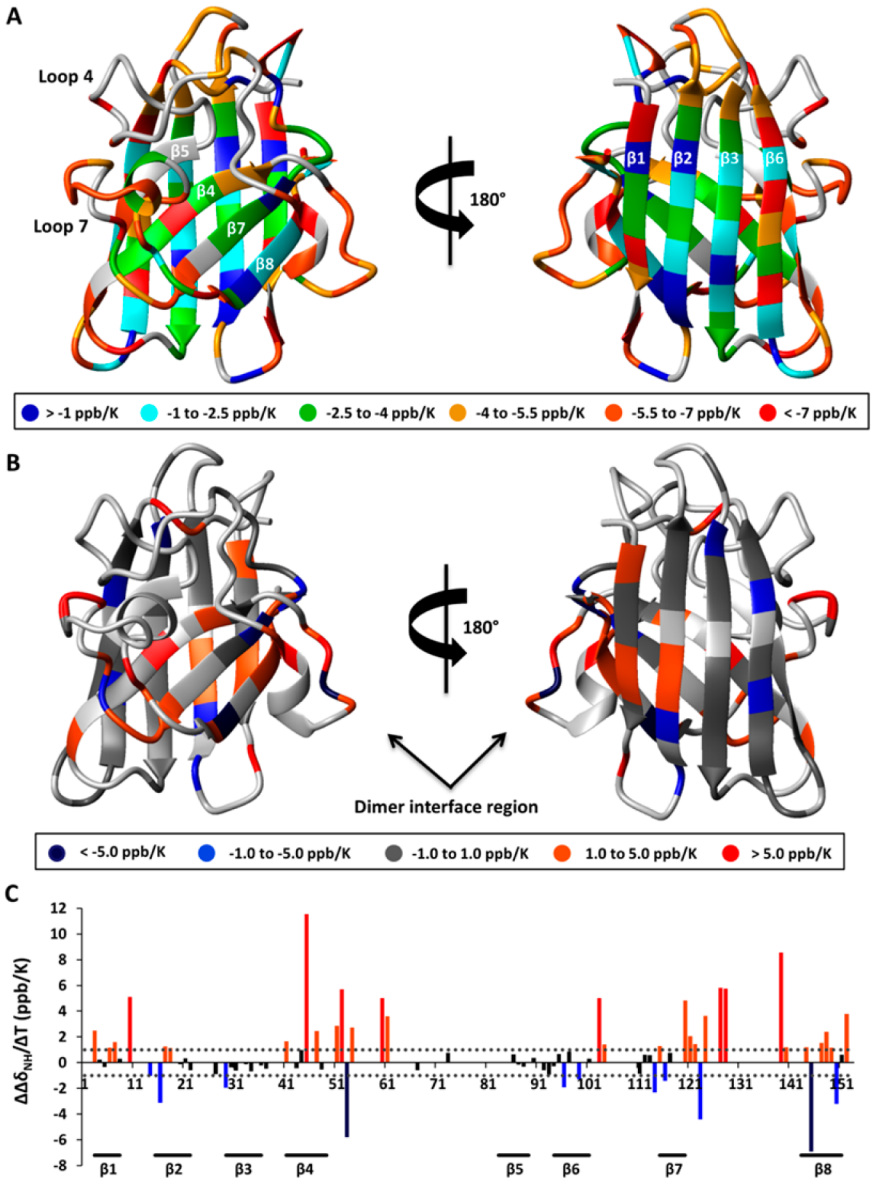

Figure 2. Changes in $\Delta\delta_{NH}/\Delta T$ for apo^{2SH} pWT relative to holo pWT SOD1. (A) $\Delta\delta_{NH}/\Delta T$ values for apo^{2SH} pWT mapped onto the 3D ribbon structure of holo pWT. The color scheme given in the legend is the same as in Figure 1B. Gray indicates residues for which no data are available. (B) Differences in $\Delta\delta_{NH}/\Delta T$ between holo pWT and apo^{2SH} pWT mapped onto the 3D ribbon structure of holo pWT ($\Delta\Delta\delta_{NH}/\Delta T = \Delta\delta_{NH}/\Delta T$ {holo pWT} $- \Delta\delta_{NH}/\Delta T$ {apo^{2SH} pWT}). A negative (positive) value indicating an amide proton with a lower (higher) propensity to become disordered with temperature in apo SOD1^{2SH} compared to holo pWT is colored blue or navy (orange or red). Values for the color scheme are given in the legend. Light gray indicates residues for which no direct comparisons can be made due to lack of data. (C) Bar chart of $\Delta\Delta\delta_{NH}/\Delta T$. Horizontal bars indicate β-strands. Relatively large values of $\Delta\Delta\delta_{NH}/\Delta T$ (greater than $\pm$1.0 ppb/K given by gray dotted lines) are colored as in (B) except that residues with changes smaller than $\pm$1.0 ppb/K are colored black.

mutants E100G and G93A have small positive values, and apo^{2SH} pWT has a large positive value. For the mutants, the $\Delta\delta_{NH}/\Delta T$ values for individual residues are for the most part very similar to pWT (Table S1), but also exhibit distinct patterns of differences (Figure 4). Because of the relatively small changes, we consider here $\Delta\Delta\delta_{NH}/\Delta T$ values greater than $\pm$0.25 ppb/K which are above the calculated experimental uncertainty in $\Delta\delta_{NH}/\Delta T$. Mutation-specific differences are described further below.

G93 is located in the solvent-exposed region known as the β-barrel plug (Figures 3D and 4A) and more specifically is a conserved residue in a tight turn that is a hotspot for ALS mutations (http://alsod.iop.kcl.ac.uk/).[38] The β-barrel plug, made up of loop 5 (which contains G93) and the adjacent loop 3, has been identified as a key stabilizing element in SOD1.[33,55] Both backbone chemical shifts and $\Delta\Delta\delta_{NH}/\Delta T$ values show residues with the most pronounced changes are clustered in the plug region (Figures 3A,D and 4A,D). Notably, in some cases (e.g., V14, G16, L38, D92, V94, and A95; Figure 4D) the magnitude of the change is similar to those observed in the much less stable apo^{2SH} pWT compared to holo pWT (Figure 2). The $\Delta\delta_{NH}/\Delta T_{avg}$ values of loops 3 and 5 are considerably more negative in G93A relative to holo pWT, suggesting that the mutation significantly reduces the structural stability of the β-barrel plug. Unexpectedly and interestingly, despite the *decrease* in global stability (Tables 1 and 2), almost half of the residues (7) with relatively larger differences in G93A appear to be *more* structured (colored blue or navy in Figure 4A, D). Overall, G93A exhibits changes that are relatively large in magnitude compared

DOI: 10.1021/acs.biochem.5b01133
Biochemistry 2016, 55, 1346−1361

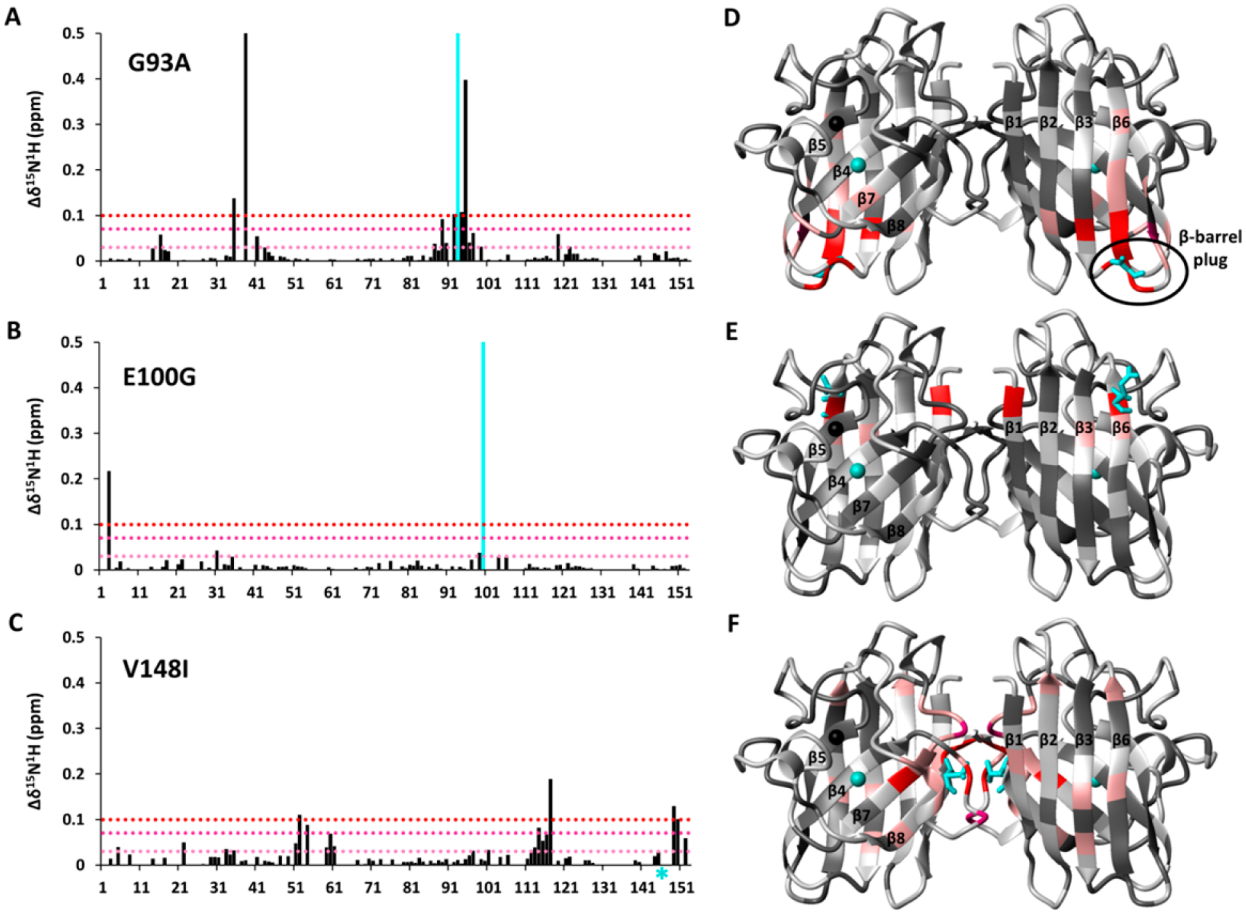

Figure 3. Backbone chemical shift changes in ALS mutant holo SOD1s relative to pWT. (A) G93A (B) E100G and (C) V148I at pH 7.8, 24 °C. Chemical shift changes, $\Delta\delta^{15}N^{1}H$, are calculated as $(\{(\Delta^{1}H)^2 + (\Delta^{15}N/5)^2)\}/2)^{1/2}$ and shown as vertical black bars (with the exception of the mutation cite which is colored cyan or given as an asterisk if no data are available). Values for the sites of mutation are off scale in (A) for residue 93 at 1.1 ppm and in (B) for residue 100 at 1.6 ppm. Chemical shift changes caused by mutations (D) G93A, (E) E100G, and (F) V148I are also mapped onto the 3D ribbon structure of pWT SOD1. The WT residue for mutations is shown in cyan in stick representation. Residues are colored to aid in visualization according to the relative magnitude of $\Delta\delta^{15}N^{1}H$ values: dark gray for values <0.03; pink for 0.03−0.07; deep pink for 0.07−0.1; red for >0.1. Light gray indicates residues where no data are available.

to those of the other mutants, propagated extensively through the structure, and indicate both increases and decreases in structural stability.

E100 is located in the charged edge strand β6 (Figures 3E and 4B); mutation from E to G decreases the net negative charge of the protein and disrupts a conserved salt bridge between E100 and K30 in β3. The largest $\Delta\delta_{NH}/\Delta T$ changes for E100G are highly localized near the site of mutation and are otherwise very small in magnitude (Figure 4B,E). Similarly, localized and minor changes in this mutant are also observed by backbone chemical shift changes (Figure 3B,E). In contrast to G93A, in E100G the $\Delta\Delta\delta_{NH}/\Delta T$ values are generally smaller, widely distributed in the protein, and are all positive (Figure 4B,E). These changes may reflect broadly propagated increased disorder relating to significantly decreased global stability (Tables 1 and 2). Relatively larger increases in $\Delta\Delta\delta_{NH}/\Delta T$ (i.e., more negative $\Delta\delta_{NH}/\Delta T$ values relative to pWT) near the site of mutation suggest a loss of stability near K30 at the end of β3 (V29 and V31) and β2 (N19 and E21). In addition, the E100G mutation may slightly increase the disorder at position 100, which appears to propagate into the following loop 6. Thus, E100G exhibits significant but limited perturbations at the site of the mutation and small relatively uniform decreases in structural stability throughout the structure.

V148 is located in β8 and its hydrophobic side chain points away from the monomer surface and is partially buried in the dimer interface (Figures 3F and 4C); mutation to I results in two larger hydrophobic residues in close proximity in the interface. Among the mutants studied here, V148I exhibits the largest number of amide protons with perturbed chemical shifts, although these are again relatively small in magnitude (Figure 3C,F). Similarly, V148I displays the largest number of residues (19) with perturbed $\Delta\delta_{NH}/\Delta T$ (Figure 4C,F). This is likely due to the central location of residue 148 in the dimer interface, a region shown to have high connectivity with distal areas of the protein structure.[56] The large majority of the $\Delta\Delta\delta_{NH}/\Delta T$ values in V148I are negative, indicating increased local structural stability, consistent with the small increase in global stability of V148I relative to pWT (Tables 1 and 2). Negative $\Delta\Delta\delta_{NH}/\Delta T$ values are observed throughout the protein, including in the dimer interface; the largest (though still small) positive values are observed for the amide protons of G114 and L117, which participate in hydrogen bonds with the carbonyl oxygens of I149 and G147, respectively, the residues flanking the mutation (Figure 4C,F). Despite these very limited observed increases in disorder surrounding the site of mutation, overall the V148I mutation appears to result in a moderate and propagating increase in structural stability.

DOI: 10.1021/acs.biochem.5b01133
Biochemistry 2016, 55, 1346−1361

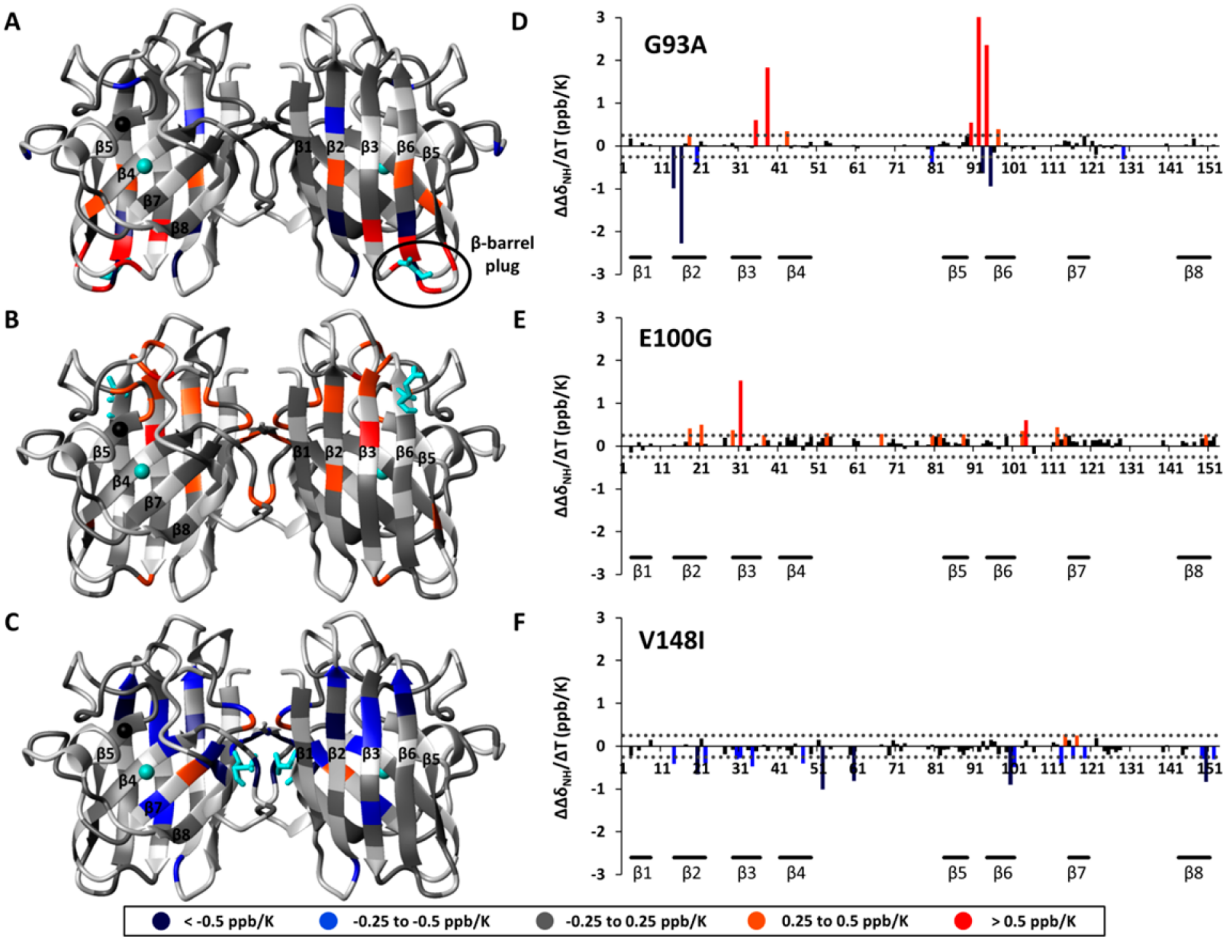

Figure 4. Changes in $\Delta\delta_{NH}/\Delta T$ for holo SOD1 mutants relative to pWT. Differences in $\Delta\delta_{NH}/\Delta T$ ($\Delta\Delta\delta_{NH}/\Delta T$) are calculated as ($\Delta\delta_{NH}/\Delta T${pWT} − $\Delta\delta_{NH}/\Delta T${mutant}). A negative (positive) value of $\Delta\Delta\delta_{NH}/\Delta T$ indicating an amide proton with a lower (higher) propensity to become disordered with temperature in the mutant relative to holo pWT is colored blue or navy (orange or red). Differences in the temperature coefficients between pWT and the ALS mutants (A) G93A, (B) E100G, and (C) V148I are colored in the 3D ribbon structure of pWT SOD1 according to values given in the legend. Light gray indicates residues for which no direct comparisons can be made due to lack of data. Bar charts of $\Delta\Delta\delta_{NH}/\Delta T$ values are shown for (D) G93A, (E) E100G, and (F) V148I. Horizontal bars indicate β-strands. Differences in $\Delta\delta_{NH}/\Delta T$ bigger than ±0.25 ppb/K (gray dotted lines) are colored as in (A−C) except that residues with changes smaller than ±0.25 ppb/K are colored black. D92 with a value of 5.91 is off scale in (D).

Curved Temperature-Dependences of δ_{NH} Show Many Residues in Holo SOD1s Populate Alternative States that are Perturbed in Common and Distinct Ways upon Mutation. The population of alternative states was characterized by fitting the curvature in δ_{NH} temperature-dependences to a quadratic equation using calculated residual chemical shift values (see Experimental Procedures).[6,20] The quadratic coefficient (a) as well as $\Delta\delta_{NH}/\Delta T$ values for the SOD1 variants studied are given in Table S1 (see Supporting Information). Representative nonlinearities are illustrated in Figure 5A, simulated for varying free-energy differences between the ground and alternative states (see Supporting Information).[20] The curvature observed experimentally for holo pWT SOD1 (Figure 5B) is comparable to that for the simulated data. In agreement with previous studies,[20] we find a correlation between the sign of curvature (i.e., concave or convex) and the value of δ_{NH} relative to random coil. This trend indicates that in most cases the alternative state is closer to random coil than the ground state and so is likely to be less structured.

From this analysis, 28 residues (~18%) in pWT exhibit curvature. These residues are spread throughout the polypeptide chain, in both β-strands and loops (Table 3). No significant correlation was observed between the magnitude of the quadratic coefficient (a) and $\Delta\delta_{NH}/\Delta T$ values for holo pWT (data not shown). It has been proposed that formation of alternative states involves local structural rearrangement with altered hydrogen bonding compared to the ground state.[20] On the basis of the crystal structure for pWT (2.5 Å; PDB 1SOS),[44] using distance and angle constraints of 2.4 Å and 35°, respectively,[57] ~59% of amide protons participate in an intramolecular hydrogen bond. A substantially larger proportion of the residues populating an alternative state are hydrogen bonded in the ground state (~86%) supporting that the alternative state may commonly be accessed through changes in hydrogen bonding.

Twelve common residues display curved temperature-dependences in holo pWT and all three mutants (Table 3; green in Figure 6A). Many of these residues are located at the junction of secondary structural elements, suggesting that a common dynamical feature of SOD1 involves disruption of native β-strand structure. There is also a cluster of residues in edge strands β5 and β6, near the β-barrel plug region, suggesting a common alternative state in all four holo proteins. These residues (A89, A95, and V97; Figure 6A) participate in hydrogen bonds that link the edge strands to the main β-sheet structure. The curvature here suggests a common alternative state where the edge strands are pulling away from the main structure near the β-barrel plug.

DOI: 10.1021/acs.biochem.5b01133
Biochemistry 2016, 55, 1346−1361

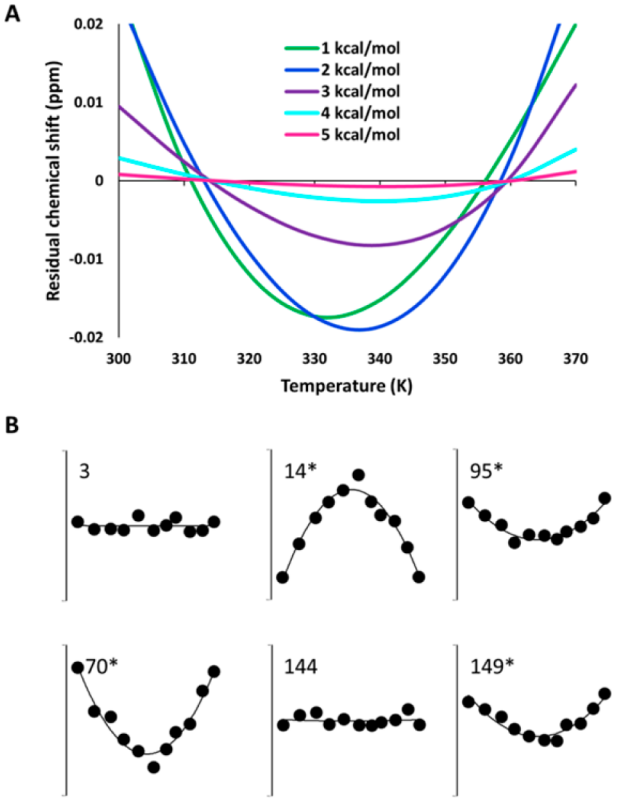

Figure 5. Curved δ_{NH} temperature-dependence of amide protons accessing an alternative state. (A) Simulation of the dependence of residual δ_{NH} versus temperature on the difference in free energy between the ground (1) and alternative (2) states for representative values of δ_1° = 8.5 ppm, g_1 = −2 ppb/K and δ_2° = 8.0 ppm, g_2 = −7 ppb/K, where δ_1° and δ_2° are the initial chemical shifts and g_1 and g_2 are the temperature coefficients of the ground and alternative states, respectively.[20] ΔS = 17.2 cal/(mol K)[102] and ΔH = 6.1, 7.1, 8.1, 9.1, and 10.1 kcal/mol corresponding to ΔG = 1, 2, 3, 4, and 5 kcal/mol, respectively. The observed chemical shift values (δ_{obs}) were calculated as described in the Supporting Information and fit using linear regression to a straight line. The residual chemical shift is the deviation from linearity ($\delta_{linfit} - \delta_{obs}$). (B) Plots of residual δ_{NH} with temperature for representative residues in holo pWT SOD1. Residual values were fit to a quadratic equation, from which the quadratic coefficient (a) was determined. The fitted curve is shown as a solid black line. Residues for which the quadratic coefficient differs from zero at $p < 0.01$ (with a ^{1}H chemical shift error of 0.005 ppm) are classified as curved (see Experimental Procedures). Plots are labeled by residue number in the top left corner. An asterisk indicates residues characterized as having a curved temperature-dependence. The vertical axis has a total range of 0.04 ppm. The horizontal axis corresponds to the temperature range 297−346 K (24−73 °C).

The curvature observed also for L38 in pWT, E100G, and V148I further supports opening of the β-barrel plug in these variants. In crystal structures of pWT SOD1[44,58] the amide proton of L38 participates in a hydrogen bond with G93 that links loops 3 and 5; however, the curvature results suggest these variants can populate an alternative conformation where that hydrogen bond is likely lost. The lack of curvature at L38 in G93A does not mean that this alternative state is not populated. Rather, a shift in $\Delta\delta_{NH}/\Delta T$ for L38 from −4.3 ppb/K in pWT to −6.1 ppb/K in G93A suggests this hydrogen bond is permanently broken in this mutant. Taken together, these results indicate a common structural fluctuation of all four holo SOD1 variants involves opening of the β-barrel plug which may expose the hydrophobic interior of the protein.

Overall, the holo mutants have a similar pattern of residues with curved temperature-dependences to pWT, but with notable differences (Table 3). For example, the two destabilized mutants, G93A and E100G, show a larger proportion of residues accessing alternative conformations, with 44 and 37 residues corresponding to ∼29% and 24%, respectively. On the other hand, the slightly more stable V148I displays an almost identical number of residues with curved δ_{NH} temperature-dependences to pWT at 29 (∼19%). Interestingly, all the mutants exhibit a larger proportion of residues accessing an alternative state in edge strand β6 and crossover loop 6 (Table 3; Figure 6). This suggests that the common conformational heterogeneity at the β5-β6 edge near the β-barrel plug described above for all four holo SOD1 variants extends further into β6 and even the following loop (6) in the mutants.

^{15}N Temperature Coefficients. In an effort to discern the still poorly understood contributing factors to ^{15}N temperature coefficients,[18,59] these were also analyzed for holo pWT. We find no correlation between the sign or magnitude of $\Delta\delta_N/\Delta T$ and amino acid or secondary structural feature (i.e., β-strand, α-helix or loop) (data not shown). There is a very weak correlation between $\Delta\delta_{NH}/\Delta T$ and $\Delta\delta_N/\Delta T$ (Figure S2), as has been observed also by others.[18] When only the magnitude of the ^{15}N temperature coefficient is considered, and not the sign, there is no longer a correlation suggesting that the sign may be of structural significance. Thus, further investigations are still needed to determine if and how $\Delta\delta_N/\Delta T$ may be used to obtain information on protein structure and dynamics.

DISCUSSION

Utility of Temperature Dependence of δ_{NH} for Characterizing Protein Structural Stability and Conformational Heterogeneity. The in-depth analyses of multiple forms of SOD1 conducted here show that the temperature-dependence of backbone amide chemical shifts is a rich source of information on both local and global protein structural stability, as well as conformational heterogeneity. To date, δ_{NH} temperature-dependences have been used mainly for assessing intramolecular hydrogen bonds, which are considered to be formed based on a simple cutoff criterion of $\Delta\delta_{NH}/\Delta T > -4.6$ ppb/K.[12,13] However, recent studies of GB1 have shown that $\Delta\delta_{NH}/\Delta T$ values are governed more generally by temperature-dependent loss of structure.[18] Similarly, a significant proportion (∼30% for pWT[44]) of the SOD1 amide protons monitored do not form intramolecular hydrogen bonds yet they display a range of stabilities comparable to that for hydrogen bonded amides, as has also been noted for other proteins.[5,12] Therefore, measuring amide proton temperature coefficients is a useful and general method to characterize the local structural stability of proteins, beyond defining just intramolecular hydrogen bonding. Following previous convention,[5,18] here we refer to a "smaller" $\Delta\delta_{NH}/\Delta T$ value when the absolute value is smaller (less negative) and a "larger" $\Delta\delta_{NH}/\Delta T$ value when the absolute value is larger (more negative), with a smaller (larger) $\Delta\delta_{NH}/\Delta T$ value indicative of increased (decreased) structural stability.

The analyses for different forms of SOD1s (apo^{2SH}, holo and mutants) show that $\Delta\delta_{NH}/\Delta T$ values provide sensitive probes of the extent of *local* structure formation which collectively reflect *overall* protein stability (Table 2). In addition, complementary information on local structural opening can be obtained by analyzing the curvature of the δ_{NH} temperature-dependence. A curved temperature-dependence can result when an amide proton is populating an alternative conformation and the relative

DOI: 10.1021/acs.biochem.5b01133
Biochemistry 2016, 55, 1346−1361

Table 3. Residues with Curved δ_{NH} Temperature Dependences in Holo SOD1 Variants[a]

Residue	1	3	5	7	9	11	13	15	17	19	21
		β1				loop 1				β2	
pWT		○ ○	● ○	○ ●		●		●	○	● ○	○ ●
G93A		○	● ●	○				●	● ○	○ ●	○ ●
E100G	○	○	● ●	●				●	○	○ ○	● ○ ●
V148I		○	○	○				●	●	○	○ ○ ● ●
Residue	**23**	**25**	**27**	**29**	**31**	**33**	**35**	**37**	**39**	**41**	**43**
		loop 2				β3			loop 3		β4
pWT			●	● ○	●	○ ○	○ ○	○	●	●	○ ○
G93A			●	● ●		○ ○	●		○ ○	●	○ ○
E100G			○	●	○ ○	○ ○	○	●	●	○	○ ○
V148I			○	● ●	○	○ ○	○	○	●	○	● ○
Residue	**45**	**47**	**49**	**51**	**53**	**55**	**57**	**59**	**61**	**63**	**65**
		β4					loop 4				
pWT	○	○ ○	○	● ●	○ ○			○	○ ○		
G93A	● ○	○ ○	○ ○	● ○	● ○	○			○ ○		
E100G	○ ○	○ ○	○	● ●	● ○				○ ○		
V148I	○	○	● ○	● ○	●	○		●	○ ○		○
Residue	**67**	**69**	**71**	**73**	**75**	**77**	**79**	**81**	**83**	**85**	**87**
				loop 4						β5	
pWT	●	● ●	○	○	○		●	○ ○	○ ●	○ ○	○ ●
G93A	●	● ●	○ ○	●	○	●	●	○ ○	○ ○	○	● ○ ●
E100G	●	● ●	○ ○	●	○	○	●	○ ○	○ ○	●	○ ○ ○
V148I	○	○ ●	○ ○	○	○	○	●	● ○	○ ○	○	○ ●
Residue	**89**	**91**	**93**	**95**	**97**	**99**	**101**	**103**	**105**	**107**	**109**
	β5	loop 5			β6				loop 6		
pWT	● ○	○	○ ○	● ○	●	○	○ ○	○	○	○	
G93A	● ○	● ○	○ ●	● ●	● ○	●	●	●	●	●	
E100G	●	● ○	○ ●	●	●	●		●	●	●	
V148I	● ○	○ ○	○ ●	○	●	●	○ ○	●	○	○ ●	
Residue	**111**	**113**	**115**	**117**	**119**	**121**	**123**	**125**	**127**	**129**	**131**
	loop 6			β7				loop 7			
pWT	○ ○	○ ○	○ ○	○	○ ●	● ○	○ ●	● ○	● ○	○	
G93A	○ ●	○ ●	● ○	○	○	● ○	○ ●	● ●	○ ○	○	
E100G	○ ●	● ○	● ○	○ ○	○ ○	● ○	○ ●	● ○	● ○		
V148I	○ ●	● ○	○ ○	○ ○	○	● ○		○ ●	○ ○		
Residue	**133**	**135**	**137**	**139**	**141**	**143**	**145**	**147**	**149**	**151**	**153**
			loop 7					β8			
pWT				○ ○		○ ○		○	○ ●	○ ○	○
G93A	○	○	○ ○	○ ○		○ ○	●	○ ●	● ○	●	○ ○
E100G			○	○ ○		○ ○	●	○	●	○ ○	○ ●
V148I				○ ○		○ ○	●		●	○	○ ○

[a]Residue numbers are given for every second residue. Residues marked with ● are curved at $p < 0.01$. Residues marked with ○ are "not curved". Where no data are available, the residue is left blank. Residue numbers for those found in β-strands are underlined.

populations of the two states are changing with temperature.[6,20] Thus, in contrast to $\Delta\delta_{NH}/\Delta T$ which is weighted heavily by and so reports on the major population (ground state) for an amide proton, curvature can report on a minor population (alternative state). It should be noted that a lack of curvature does not prove the absence of an alternative state for a particular amide proton. Rather, if the energy difference between the two states is too large (Figure 5A), or the ground and alternative state have very similar δ_{NH} or $\Delta\delta_{NH}/\Delta T$, or the amide proton is in exchange with a large number of alternative conformations, a net linear temperature-

DOI: 10.1021/acs.biochem.5b01133
Biochemistry 2016, 55, 1346−1361

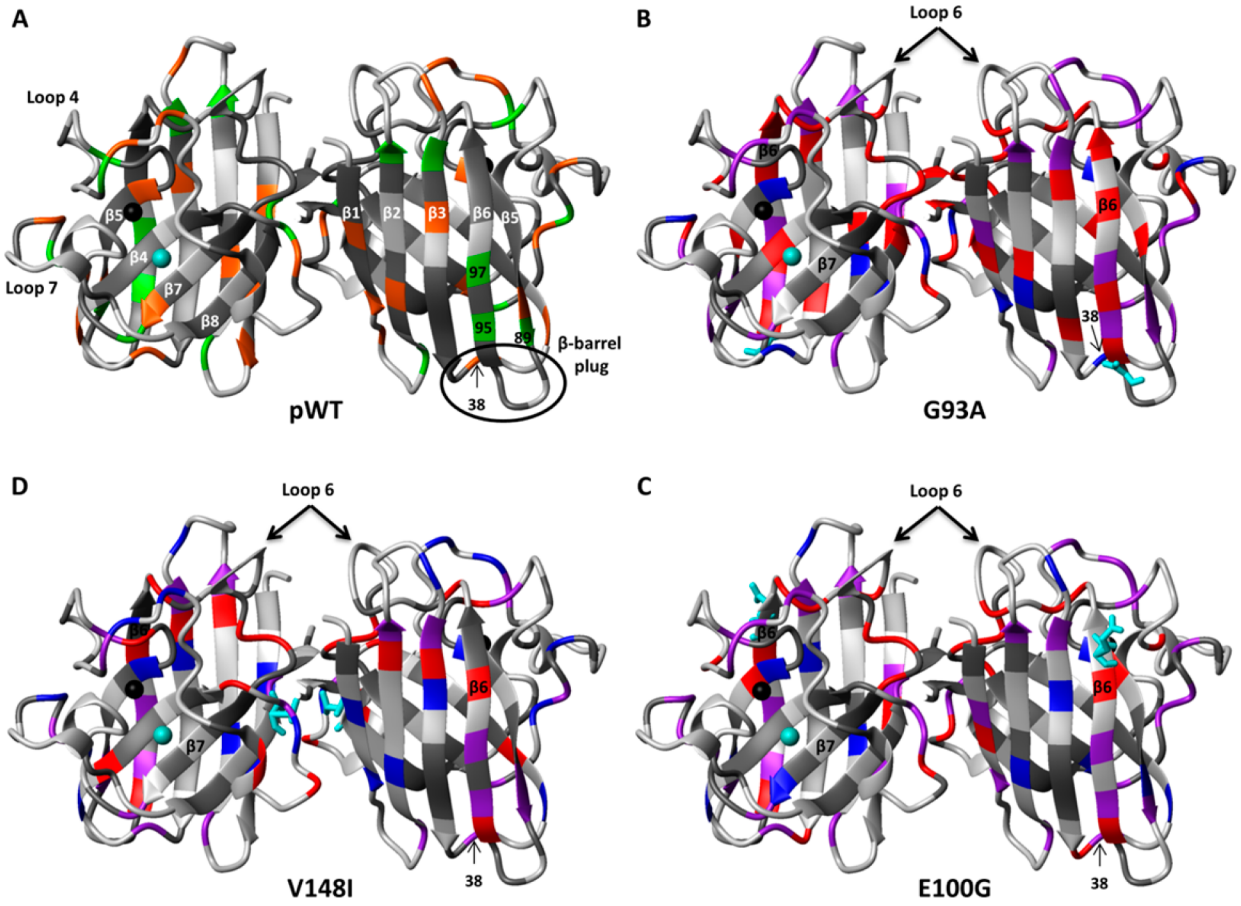

Figure 6. Ribbon structure highlighting structural fluctuations in holo pWT SOD1 and mutants revealed from curved δ_{NH} temperature-dependences. (A) Residues accessing an alternative state in all four holo variants (pWT, G93A, E100G, and V148I) are colored green. The curvature at A89, A95, and V97 in all four variants suggests a common alternative state where the edge strands (β5-β6) may be pulling away from the main structure near the β-barrel plug (residue numbers are given on the ribbon). Additional residues accessing an alternative state in pWT are colored orange. Residues colored orange may also access an alternative state in some but not all of the mutants. Residues accessing an alternative state in mutants (B) G93A, (C) E100G, and (D) V148I compared to pWT are given by a different color scheme. Blue indicates residues where access to an alternative state is observed in pWT but not the mutant. Purple indicates residues where access to an alternative state is observed in both mutant and pWT. Red indicates residues where access to an alternative state is observed in the mutant but not pWT. Dark gray indicates residues that do not exhibit curvature in mutant or pWT. Light gray indicates residues where no direct comparison can be made due to limited data. The destabilized mutants, G93A and E100G, display a larger number of residues accessing alternative states compared to the slightly stabilized V148I which has a comparable number to pWT. All of the mutants have a larger proportion of residues accessing an alternative state in β6 and loop 6. The total number of residues identified to be accessing an alternative state in holo pWT, G93A, E100G and V148I is 28 (18%), 44 (29%), 37 (24%), and 19 (19%), respectively.

dependence may be observed.[6] Therefore, the number of residues identified as accessing an alternative state likely represents a minimum. Nevertheless, the curvature measurements for holo SOD1 variants here provide evidence for widespread and varying conformational heterogeneity even in these very stable proteins (Table 3, Figure 6).

In the following discussion, we consider first how the δ_{NH} temperature-dependence data relate to other studies of folding and dynamics for SOD1, followed by implications for SOD1 misfolding in ALS and general aspects of protein folding and dynamics.

Structural Fluctuations in Holo pWT SOD1. The analyses of the temperature-dependence of δ_{NH}'s provide evidence for considerable variation in local structural stability and conformational heterogeneity in holo pWT SOD1. Under conditions favoring the folded state, the observable temperature-induced changes include fraying at the ends of β-strands, local unfolding at the β5-β6 edge and loss of structural integrity near the dimer interface, indicating that holo pWT SOD1 loses structure with temperature first at the periphery of the protein (Figure 1). Further, under equilibrium conditions at least 18% of residues show evidence for population of low-energy alternative states (Table 3, Figure 6A), which may be important for enzymatic activity.[4] Thus, despite its extremely high global thermodynamic stability, holo SOD1 exhibits significant mobility, highlighting how global stability is not always a reliable predictor of protein flexibility and motion, as is also apparent from studies of other proteins characterized by the temperature-dependence of δ_{NH}s.[6,17,20,22] Similarly, a lack of correlation between global protein stability and dynamics has also been observed using other methods.[60−62]

Distinct Local Changes Determine Global Stability Changes upon Maturation and Mutation. The overall picture that emerges from the measurements of δ_{NH} with temperature for SOD1s is that while the *average* changes related to maturation state or mutation are correlated with changes in global protein stability, unique differences are observed at high resolution. The different global stabilities of the different SOD1s are mirrored in the average and spread of $\Delta\delta_{NH}/\Delta T$ values (Table 2). Also, the overall effects of mutations on the near-

DOI: 10.1021/acs.biochem.5b01133
Biochemistry 2016, 55, 1346−1361

native state dynamics of SOD1 measured by curvature correlate with global stability, with the destabilized mutants (G93A and E100G) displaying a larger proportion of residues accessing low free-energy alternative states (>24%) and the slightly stabilized mutant (V148I) displaying a nearly identical proportion to pWT (19%; Table 3). The underlying molecular basis for the global stability changes is revealed by temperature-dependence analyses for individual amide protons for the different SOD1s, considered further below.

apo^{2SH} pWT. The average value of $\Delta\delta_{NH}/\Delta T$ for apo^{2SH} pWT is notably large (more negative) compared to those for other more stable proteins.[5] Compared to holo pWT, $\Delta\delta_{NH}/\Delta T$ measurements reveal that structural stability is greatly reduced in apo^{2SH}, particularly in the C-terminal β-sheet and the long loops 4 and 7 (Table 2, Figure 2), regions important for metal binding and dimerization. Increased mobility in all three of these regions has also been observed by ^{15}N relaxation measurements of the apo monomer[52] and estimates by RCI of *apo*^{2SH},[16] as well as computational modeling of the apo monomer.[54,63,64] These various NMR and modeling findings are also consistent with the low extent of structure measured directly by crystallography and NMR for apo^{2SH} (or the apo cysteine free variant[65]) compared to holo pWT[16,52] and by the difference in global stabilities determined by calorimetry and chemical denaturation.[36,37,66] A relatively low change in heat capacity for unfolding (ΔC_p) also indicates the immature monomeric apo^{2SH} is expanded compared to more mature forms of the protein.[51] Thus, the $\Delta\delta_{NH}/\Delta T$ results for apo^{2SH} pWT are consistent with many other results and provide valuable complementary information on structural stability at high resolution for the immature form of the protein, which has been challenging to define using traditional methods owing to its highly dynamic properties.

Holo Mutants. For the holo SOD1 mutants, $\Delta\delta_{NH}/\Delta T$ values differ markedly in comparison to pWT. For G93A, altered local structural stabilities are the most pronounced, with large changes near the site of mutation in the β-barrel plug, and smaller changes propagating quite extensively through the protein (Figure 4A,D). A similar pattern is observed by backbone chemical shift changes (Figure 3A,D), and overall the proportion of residues exhibiting conformational heterogeneity is increased in the mutant (Figure 6B, Table 3). Previous amide exchange and backbone relaxation studies of G93A also highlight increased disorder in the β-barrel plug.[49,67,68] The location of the mutation in a loop at the protein surface, and the lower structural stability of the adjacent β5 and β6 strands at the periphery of the structure (Figure 1) likely allow changes, in stability, structure, and dynamics, to be transmitted through the protein.

E100G exhibits very different variation of δ_{NH} with temperature than G93A (Figures 4B,E and 6C), despite having similar global stability (Tables 1 and 2). The small magnitudes of changes in backbone chemical shifts (Figure 3B,E), $\Delta\Delta\delta_{NH}/\Delta T$ (Figure 4B,E) and amide exchange rates[49] show little evidence for perturbation of structure in E100G, even though its global stability is slightly *lower* than G93A, i.e., significantly decreased (Table 2). Conformational changes may be limited by the location of this mutation at the opposite (C-terminal) end of the β6 strand relative to G93, in a region that appears to be well anchored to the rest of the barrel. Nevertheless, overall the conformational heterogeneity in E100G is increased (Figure 6C, Table 3), and small but extensive positive $\Delta\Delta\delta_{NH}/\Delta T$ values indicate destabilization is propagated throughout most of the protein (Figure 4E). This suggests that the inability of the protein structure to relax locally near the mutation site results in more subtle, long-range decreases in stability.

For V148I, another distinct pattern of changes in $\Delta\delta_{NH}/\Delta T$ is observed; there are small increases in structural stability for many amide protons throughout the protein with very limited decreases immediately adjacent to the mutation (Figure 4C,F) and an altered pattern but no net increases in residues exhibiting conformational heterogeneity (Figure 6D, Table 3). Previous studies of disulfide reduced and oxidized apo forms of V148I have shown that this mutation increases monomer stability and modestly weakens the dimer interface.[37,69,70] Also, stability measurements have shown that metal binding increases the affinity of the SOD1 dimer interface.[35,36,54] It is not clear from the available data whether the dimer interface is weakened in holo V148I but, based on the widespread increases in structural stability through the protein, the increased global stability likely arises at least in part from increased monomer stability.

Interestingly, all three mutants display increased conformational heterogeneity relative to pWT in β6 and crossover loop 6, which runs from the outside edge of the protein into the dimer interface (Figure 6). Increased flexibility in β6 compared to pWT has also been observed in G37R and G93A by computational simulations and backbone relaxation experiments, respectively.[64,68] We have recently found using isothermal titration that in the apo form of SOD1 many mutations, including ones far from the dimer interface, weaken the interface stability.[69] Computational studies suggest that this occurs for the majority of ALS-associated mutations in SOD1[71] and may be related to changes in long-range dynamics coupling the dimer interface to the rest of the protein which are disrupted upon mutation.[56] Similarly, recent analyses of protein structures and simulations have provided evidence for the transfer of structural information across β-sheets via correlated backbone motions.[72] The increased dynamics in loop 6 revealed by the curvature analysis may represent a common path by which mutations can exert an effect on the dimer interface. Taken together, the temperature-dependences of δ_{NH} analyses are a valuable complement to other studies and help define experimentally at high resolution the paths by which changes in local stability and dynamics are communicated through SOD1.

Implications for ALS − Variable Extent of "Rescue" of Mutants to WT-like Properties by Metalation. Overall, the consequences of mutation observed here for the holo form of SOD1 suggest that metal binding can maintain various SOD1 mutants in a stable, WT-like state, with complex changes in stability and dynamics that vary extensively with mutation. Measurements of global thermodynamic stability have shown that the effects of mutations are usually larger in apo than in holo SOD1s.[35−37,73−76] Other investigations of SOD1 dynamics by NMR have shown that the extent to which metal binding promotes structure formation varies with mutation. For example, metal binding was reported to almost completely restore the ps−ns dynamics of G37R to that of WT and the tendency of the mutant to self-associate in solution was indistinguishable from pWT. In contrast, G93A exhibits localized increases in backbone mobility compared to WT, and S134N has even larger changes in dynamics and increased self-association.[68,77,78]

Despite extensive research, the mechanisms of SOD1 aggregation and the forms of the protein from which aggregation arises remain unclear. Though holo SOD1 is highly abundant in cells,[79] it is generally thought not to aggregate due to its very high stability.[41,46,51] On the other hand, over time under physiologically relevant conditions holo SOD1, even in the absence of

DOI: 10.1021/acs.biochem.5b01133
Biochemistry 2016, 55, 1346−1361

mutation, can undergo changes in metalation and/or dimerization resulting in low levels of aggregation.[80] Other studies have suggested immature monomeric SOD1 may play a key role in disease by readily initiating aggregation and recruiting more mature forms to aggregate.[81,82] The present studies reveal conformational heterogeneity surrounding the Zn^{2+}-binding site in holo pWT and mutants (Figure 6) suggesting that Zn^{2+} loss may be a common pathway giving rise to mismetalation, as also suggested by kinetic experiments.[66,83] The altered structural stability and/or conformational dynamics in the mutants could promote metal loss and misfolding, altered interactions with other cellular components and/or lead to aberrant enzymatic activity. However, since the present data do not provide any structural information about the low lying conformers, we cannot ascertain whether the detected structural fluctuations will be directly related to aggregation prone states. Nevertheless, the results herein are pertinent to addressing a key outstanding challenge in the field of protein conformational disorders, which is to determine how different molecular mechanisms of aggregation for the same or different protein variants may be identified and ultimately treated. The present findings support the general hypothesis that while holo SOD1 usually does not directly aggregate, changes in its stability and dynamics may contribute to aggregation in ways that can vary considerably with mutation.[41]

General Implications of Temperature-Dependence of δ_{NH} Measurements for Defining Protein Energetics. A particularly interesting result of the current studies is the propagating *increases* as well as decreases in structural stability measured by $\Delta\delta_{NH}/\Delta T$ that are clearly evident in apo^{2SH} pWT and holo G93A proteins compared to the more stable holo pWT (Figure 2B,C; Figure 4A,D). Thus, comparisons of $\Delta\delta_{NH}/\Delta T$ can provide a valuable high resolution tool for elucidating how changes in local stability determine global changes. Modes of structural relaxation and entropy-enthalpy compensation within a protein are central to understanding changes in protein energetics upon ligand binding and mutation, which remain difficult to predict accurately.[84−88]

Recently, there has been intense research on quantifying the contributions to protein−ligand binding energetics of protein conformational entropy using ^{15}N relaxation measurements, which typically show concomitant increases as well as decreases of mobility within the protein upon ligand binding.[84−86] To date, analogous changes in protein flexibility for changes in stability caused by mutation have been little remarked upon.[88,89] However, such effects have been observed,[89,90] including in ^{15}N relaxation measurements of holo G93A.[68] In the case of G93A, there is little correspondence at the level of individual residues between changes in ps-ns time scale dynamics measured by ^{15}N relaxation and the results measured here; however, in both types of measurements increases and decreases are observed, in particular, close to the site of mutation, as well as for more distant residues. In addition, there has been exciting progress recently in modeling and predicting relationships between chemical shifts and protein structure at high resolution.[91,92] This may be further developed to elucidate the nature of changes in structure and energetics with temperature.

The results described herein indicate that the temperature-dependences of δ_{NH} can be highly sensitive reporters of both local structural stability and conformational heterogeneity; another attractive feature is that they can be measured and analyzed relatively easily. Interestingly, for both holo and reduced apo SOD1 there is no clear correlation between $\Delta\delta_{NH}/\Delta T$ (Table S1) and order parameters estimated from chemical shifts[16] using RCI,[53] indicating regions in SOD1 that lose structure with increasing temperature are not necessarily those that are most flexible at equilibrium. Although temperature-dependences of δ_{NH} have been little used to date for investigating changes caused by ligand binding or mutations, they may be particularly useful for testing and improving computational modeling[22,91−95] to elucidate differences in related forms proteins, such as to understand the molecular mechanisms underlying protein misfolding and aggregation in disease.[39,40,96−98]

■ ASSOCIATED CONTENT

Supporting Information

The Supporting Information is available free of charge on the ACS Publications website at DOI: 10.1021/acs.biochem.5b01133.

Figure S1: The fraction of globally unfolded holo SOD1 as a function of temperature calculated for a typical NMR sample protein concentration of 30 mg mL^{-1}. Figure S2: Correlation of $\Delta\delta_{NH}/\Delta T$ and $\Delta\delta_N/\Delta T$ for holo pWT SOD1 at pH 7.8. SI Text: Theoretical model for curved δ_{NH} temperature-dependence. Table S1: Amide proton temperature coefficients ($\Delta\delta_{NH}/\Delta T$) and quadratic coefficient (a) of residues with curved δ_{NH} temperature-dependences for SOD1 variants. (PDF)

■ AUTHOR INFORMATION

Corresponding Author

*E-mail: meiering@uwaterloo.ca. Phone: (519) 888-4567 ext. 32254.

Funding

This work was supported by the Canadian Institutes of Health Research (CIHR).

Notes

The authors declare no competing financial interest.

■ ACKNOWLEDGMENTS

We are grateful to Jan Venne for technical assistance with the NMR experiments and to Duncan Mackenzie for all the perceptive discussions.

■ ABBREVIATIONS

ALS, amyotrophic lateral sclerosis; apo^{2SH}, monomeric unmetalated and disulfide-reduced SOD1; CARA, computer aided resonance assignment; HEPES, hydroxyethyl piperazine *N*′-2-ethanesulfonic acid; holo SOD1, fully metalated dimeric SOD1; pWT, pseudo wild-type (C6A/C111S) SOD1; SOD1, human Cu, Zn superoxide dismutase; β, $\Delta H_{vH}/\Delta H_{cal}$ × molecular weight of the SOD1 homodimer; ΔC_p, change in specific heat capacity upon unfolding; ΔG, change in Gibbs free energy of unfolding; Δh, specific enthalpy of unfolding; ΔH_{cal}, calorimetric enthalpy of unfolding; ΔH_{vH}, van't Hoff enthalpy of unfolding; δ_{NH}, amide proton chemical shift; $\Delta\delta_{NH}/\Delta T$, amide proton temperature coefficient; $\Delta\delta_{NH}/\Delta T_{avg}$, average amide proton temperature coefficient for secondary structural element; $\Delta\Delta\delta_{NH}/\Delta T$, difference in amide proton temperature coefficient; $\Delta\delta_N/\Delta T$, backbone amide ^{15}N temperature coefficient; $\Delta\delta^{15}N^1H$, weighted average difference in backbone amide chemical shift of mutant SOD1 relative to pWT

DOI: 10.1021/acs.biochem.5b01133
Biochemistry 2016, 55, 1346−1361

REFERENCES

(1) Cooper, A., and Dryden, D. T. (1984) Allostery without conformational change. A plausible model. *Eur. Biophys. J. 11*, 103−109.
(2) Peng, J. W. (2012) Exposing the Moving Parts of Proteins with NMR Spectroscopy. *J. Phys. Chem. Lett. 3*, 1039−1051.
(3) Perica, T., Marsh, J. A., Sousa, F. L., Natan, E., Colwell, L. J., Ahnert, S. E., and Teichmann, S. A. (2012) The emergence of protein complexes: quaternary structure, dynamics and allostery. Colworth Medal Lecture. *Biochem. Soc. Trans. 40*, 475−491.
(4) Wand, A. J., Moorman, V. R., and Harpole, K. W. (2013) A surprising role for conformational entropy in protein function. *Top. Curr. Chem. 337*, 69−94.
(5) Andersen, N. H., Neidigh, J. W., Harris, S. M., Lee, G. M., Liu, Z., and Tong, H. (1997) Extracting Information from the Temperature Gradients of Polypeptide NH Chemical Shifts. 1. The Importance of Conformational Averaging. *J. Am. Chem. Soc. 119*, 8547−8561.
(6) Baxter, N. J., Hosszu, L. L., Waltho, J. P., and Williamson, M. P. (1998) Characterisation of low free-energy excited states of folded proteins. *J. Mol. Biol. 284*, 1625−1639.
(7) Baxter, N. J., and Williamson, M. P. (1997) Temperature dependence of 1H chemical shifts in proteins. *J. Biomol. NMR 9*, 359−369.
(8) Bouvignies, G., Vallurupalli, P., Cordes, M. H., Hansen, D. F., and Kay, L. E. (2011) Measuring 1HN temperature coefficients in invisible protein states by relaxation dispersion NMR spectroscopy. *J. Biomol. NMR 50*, 13−18.
(9) Campos, L. A., Sadqi, M., Liu, J., Wang, X., English, D. S., and Munoz, V. (2013) Gradual disordering of the native state on a slow two-state folding protein monitored by single-molecule fluorescence spectroscopy and NMR. *J. Phys. Chem. B 117*, 13120−13131.
(10) Chandra, K., Sharma, Y., and Chary, K. V. (2011) Characterization of low-energy excited states in the native state ensemble of non-myristoylated and myristoylated neuronal calcium sensor-1. *Biochim. Biophys. Acta, Proteins Proteomics 1814*, 334−344.
(11) Cho, M. K., Xiang, S., Kim, H. Y., Becker, S., and Zweckstetter, M. (2012) Cold-induced changes in the protein ubiquitin. *PLoS One 7*, e37270.
(12) Cierpicki, T., and Otlewski, J. (2001) Amide proton temperature coefficients as hydrogen bond indicators in proteins. *J. Biomol. NMR 21*, 249−261.
(13) Cierpicki, T., Zhukov, I., Byrd, R. A., and Otlewski, J. (2002) Hydrogen bonds in human ubiquitin reflected in temperature coefficients of amide protons. *J. Magn. Reson. 157*, 178−180.
(14) Kjaergaard, M., Norholm, A. B., Hendus-Altenburger, R., Pedersen, S. F., Poulsen, F. M., and Kragelund, B. B. (2010) Temperature-dependent structural changes in intrinsically disordered proteins: formation of alpha-helices or loss of polyproline II? *Protein Sci. 19*, 1555−1564.
(15) Naganathan, A. N., and Munoz, V. (2014) Thermodynamics of downhill folding: multi-probe analysis of PDD, a protein that folds over a marginal free energy barrier. *J. Phys. Chem. B 118*, 8982−8994.
(16) Sekhar, A., Rumfeldt, J. A., Broom, H. R., Doyle, C. M., Bouvignies, G., Meiering, E. M., and Kay, L. E. (2015) Thermal fluctuations of immature SOD1 lead to separate folding and misfolding pathways. *eLife 4*, e07296.
(17) Srivastava, A. K., and Chary, K. V. (2011) Conformational heterogeneity and dynamics in a betagamma-Crystallin from Hahella chejuensis. *Biophys. Chem. 157*, 7−15.
(18) Tomlinson, J. H., and Williamson, M. P. (2012) Amide temperature coefficients in the protein G B1 domain. *J. Biomol. NMR 52*, 57−64.
(19) Tunnicliffe, R. B., Waby, J. L., Williams, R. J., and Williamson, M. P. (2005) An experimental investigation of conformational fluctuations in proteins G and L. *Structure 13*, 1677−1684.
(20) Williamson, M. P. (2003) Many residues in cytochrome c populate alternative states under equilibrium conditions. *Proteins: Struct., Funct., Genet. 53*, 731−739.
(21) Yao, S., Young, I. G., Norton, R. S., and Murphy, J. M. (2011) Murine interleukin-3: structure, dynamics, and conformational heterogeneity in solution. *Biochemistry 50*, 2464−2477.
(22) Dellarole, M., Caro, J. A., Roche, J., Fossat, M., Barthe, P., Garcia-Moreno, E. B., Royer, C. A., and Roumestand, C. (2015) Evolutionarily Conserved Pattern of Interactions in a Protein Revealed by Local Thermal Expansion Properties. *J. Am. Chem. Soc. 137*, 9354−9362.
(23) Hong, J., Jing, Q., and Yao, L. (2013) The protein amide (1)H(N) chemical shift temperature coefficient reflects thermal expansion of the N-H···O═C hydrogen bond. *J. Biomol. NMR 55*, 71−78.
(24) Ohnishi, M., and Urry, D. W. (1969) Temperature dependence of amide proton chemical shifts: the secondary structures of gramicidin S and valinomycin. *Biochem. Biophys. Res. Commun. 36*, 194−202.
(25) Rothemund, S., Weisshoff, H., Beyermann, M., Krause, E., Bienert, M., Mugge, C., Sykes, B. D., and Sonnichsen, F. D. (1996) Temperature coefficients of amide proton NMR resonance frequencies in trifluoroethanol: a monitor of intramolecular hydrogen bonds in helical peptides. *J. Biomol. NMR 8*, 93−97.
(26) Clore, G. M. (2011) Exploring sparsely populated states of macromolecules by diamagnetic and paramagnetic NMR relaxation. *Protein Sci. 20*, 229−246.
(27) Fawzi, N. L., Ying, J., Ghirlando, R., Torchia, D. A., and Clore, G. M. (2011) Atomic-resolution dynamics on the surface of amyloid-beta protofibrils probed by solution NMR. *Nature 480*, 268−272.
(28) Nikolova, E. N., Kim, E., Wise, A. A., O'Brien, P. J., Andricioaei, I., and Al-Hashimi, H. M. (2011) Transient Hoogsteen base pairs in canonical duplex DNA. *Nature 470*, 498−502.
(29) Palmer, A. G., 3rd, Kroenke, C. D., and Loria, J. P. (2001) Nuclear magnetic resonance methods for quantifying microsecond-to-millisecond motions in biological macromolecules. *Methods Enzymol. 339*, 204−238.
(30) Sekhar, A., and Kay, L. E. (2013) NMR paves the way for atomic level descriptions of sparsely populated, transiently formed biomolecular conformers. *Proc. Natl. Acad. Sci. U. S. A. 110*, 12867−12874.
(31) Vallurupalli, P., Bouvignies, G., and Kay, L. E. (2012) Studying "invisible" excited protein states in slow exchange with a major state conformation. *J. Am. Chem. Soc. 134*, 8148−8161.
(32) Krishna, M. M., Hoang, L., Lin, Y., and Englander, S. W. (2004) Hydrogen exchange methods to study protein folding. *Methods 34*, 51−64.
(33) Tainer, J. A., Getzoff, E. D., Beem, K. M., Richardson, J. S., and Richardson, D. C. (1982) Determination and analysis of the 2 A-structure of copper, zinc superoxide dismutase. *J. Mol. Biol. 160*, 181−217.
(34) Lepock, J. R., Frey, H. E., and Hallewell, R. A. (1990) Contribution of conformational stability and reversibility of unfolding to the increased thermostability of human and bovine superoxide dismutase mutated at free cysteines. *J. Biol. Chem. 265*, 21612−21618.
(35) Rumfeldt, J. A., Stathopulos, P. B., Chakrabarrty, A., Lepock, J. R., and Meiering, E. M. (2006) Mechanism and thermodynamics of guanidinium chloride-induced denaturation of ALS-associated mutant Cu,Zn superoxide dismutases. *J. Mol. Biol. 355*, 106−123.
(36) Stathopulos, P. B., Rumfeldt, J. A., Karbassi, F., Siddall, C. A., Lepock, J. R., and Meiering, E. M. (2006) Calorimetric analysis of thermodynamic stability and aggregation for apo and holo amyotrophic lateral sclerosis-associated Gly-93 mutants of superoxide dismutase. *J. Biol. Chem. 281*, 6184−6193.
(37) Vassall, K. A., Stubbs, H. R., Primmer, H. A., Tong, M. S., Sullivan, S. M., Sobering, R., Srinivasan, S., Briere, L. A., Dunn, S. D., Colon, W., and Meiering, E. M. (2011) Decreased stability and increased formation of soluble aggregates by immature superoxide dismutase do not account for disease severity in ALS. *Proc. Natl. Acad. Sci. U. S. A. 108*, 2210−2215.
(38) Abel, O., Shatunov, A., Jones, A. R., Andersen, P. M., Powell, J. F., and Al-Chalabi, A. (2013) Development of a Smartphone App for a Genetics Website: The Amyotrophic Lateral Sclerosis Online Genetics Database (ALSoD). *JMIR Mhealth Uhealth 1*, e18.
(39) Robberecht, W., and Philips, T. (2013) The changing scene of amyotrophic lateral sclerosis. *Nat. Rev. Neurosci. 14*, 248−264.

DOI: 10.1021/acs.biochem.5b01133
Biochemistry 2016, 55, 1346−1361

(40) Soto, C., and Estrada, L. D. (2008) Protein misfolding and neurodegeneration. *Arch. Neurol. 65*, 184−189.
(41) Broom, H. R., Rumfeldt, J. A., and Meiering, E. M. (2014) Many roads lead to Rome? Multiple modes of Cu,Zn superoxide dismutase destabilization, misfolding and aggregation in amyotrophic lateral sclerosis. *Essays Biochem. 56*, 149−165.
(42) Hallewell, R. A., Imlay, K. C., Lee, P., Fong, N. M., Gallegos, C., Getzoff, E. D., Tainer, J. A., Cabelli, D. E., Tekamp-Olson, P., Mullenbach, G. T., et al. (1991) Thermostabilization of recombinant human and bovine CuZn superoxide dismutases by replacement of free cysteines. *Biochem. Biophys. Res. Commun. 181*, 474−480.
(43) McRee, D. E., Redford, S. M., Getzoff, E. D., Lepock, J. R., Hallewell, R. A., and Tainer, J. A. (1990) Changes in crystallographic structure and thermostability of a Cu,Zn superoxide dismutase mutant resulting from the removal of a buried cysteine. *J. Biol. Chem. 265*, 14234−14241.
(44) Parge, H. E., Hallewell, R. A., and Tainer, J. A. (1992) Atomic structures of wild-type and thermostable mutant recombinant human Cu,Zn superoxide dismutase. *Proc. Natl. Acad. Sci. U. S. A. 89*, 6109−6113.
(45) Getzoff, E. D., Cabelli, D. E., Fisher, C. L., Parge, H. E., Viezzoli, M. S., Banci, L., and Hallewell, R. A. (1992) Faster superoxide dismutase mutants designed by enhancing electrostatic guidance. *Nature 358*, 347−351.
(46) Stathopulos, P. B., Rumfeldt, J. A., Scholz, G. A., Irani, R. A., Frey, H. E., Hallewell, R. A., Lepock, J. R., and Meiering, E. M. (2003) Cu/Zn superoxide dismutase mutants associated with amyotrophic lateral sclerosis show enhanced formation of aggregates in vitro. *Proc. Natl. Acad. Sci. U. S. A. 100*, 7021−7026.
(47) Hindman, J. C. (1966) Proton Resonance Shift of Water in the Gas and Liquid States. *J. Chem. Phys. 44*, 4582−4592.
(48) Keller, R. (2004) The Computer Aided Resonance Assignment Tutorial, Cantina Verlag, Goldau.
(49) Rumfeldt, J. A. (2006) Thermodynamics, Kinetics and Structural Dynamics of Amyotrophic Lateral Sclerosis-Associated Mutant Copper-Zinc Superoxide Dismutase In *Chemistry*; University of Waterloo, Waterloo.
(50) Sturtevant, J. M. (1987) Biochemical applications of differential scanning calorimetry. *Annu. Rev. Phys. Chem. 38*, 463−488.
(51) Doyle, C. M., Rumfeldt, J. A., Broom, H. R., Broom, A., Stathopulos, P. B., Vassall, K. A., Almey, J. J., and Meiering, E. M. (2013) Energetics of oligomeric protein folding and association. *Arch. Biochem. Biophys. 531*, 44−64.
(52) Banci, L., Bertini, I., Cramaro, F., Del Conte, R., Rosato, A., and Viezzoli, M. S. (2000) Backbone dynamics of human Cu,Zn superoxide dismutase and of its monomeric F50E/G51E/E133Q mutant: the influence of dimerization on mobility and function. *Biochemistry 39*, 9108−9118.
(53) Berjanskii, M. V., and Wishart, D. S. (2008) Application of the random coil index to studying protein flexibility. *J. Biomol. NMR 40*, 31−48.
(54) Ding, F., and Dokholyan, N. V. (2008) Dynamical roles of metal ions and the disulfide bond in Cu, Zn superoxide dismutase folding and aggregation. *Proc. Natl. Acad. Sci. U. S. A. 105*, 19696−19701.
(55) Deng, H. X., Hentati, A., Tainer, J. A., Iqbal, Z., Cayabyab, A., Hung, W. Y., Getzoff, E. D., Hu, P., Herzfeldt, B., Roos, R. P., et al. (1993) Amyotrophic lateral sclerosis and structural defects in Cu,Zn superoxide dismutase. *Science 261*, 1047−1051.
(56) Khare, S. D., and Dokholyan, N. V. (2006) Common dynamical signatures of familial amyotrophic lateral sclerosis-associated structurally diverse Cu, Zn superoxide dismutase mutants. *Proc. Natl. Acad. Sci. U. S. A. 103*, 3147−3152.
(57) Berndt, K. D., Guntert, P., and Wuthrich, K. (1993) Nuclear magnetic resonance solution structure of dendrotoxin K from the venom of Dendroaspis polylepis polylepis. *J. Mol. Biol. 234*, 735−750.
(58) Strange, R. W., Antonyuk, S., Hough, M. A., Doucette, P. A., Rodriguez, J. A., Hart, P. J., Hayward, L. J., Valentine, J. S., and Hasnain, S. S. (2003) The structure of holo and metal-deficient wild-type human Cu, Zn superoxide dismutase and its relevance to familial amyotrophic lateral sclerosis. *J. Mol. Biol. 328*, 877−891.
(59) Farber, P., Darmawan, H., Sprules, T., and Mittermaier, A. (2010) Analyzing protein folding cooperativity by differential scanning calorimetry and NMR spectroscopy. *J. Am. Chem. Soc. 132*, 6214−6222.
(60) Gobeil, S. M., Clouthier, C. M., Park, J., Gagne, D., Berghuis, A. M., Doucet, N., and Pelletier, J. N. (2014) Maintenance of native-like protein dynamics may not be required for engineering functional proteins. *Chem. Biol. 21*, 1330−1340.
(61) Hernandez, G., Jenney, F. E., Jr., Adams, M. W., and LeMaster, D. M. (2000) Millisecond time scale conformational flexibility in a hyperthermophile protein at ambient temperature. *Proc. Natl. Acad. Sci. U. S. A. 97*, 3166−3170.
(62) Smith, M. T., Meissner, J., Esmonde, S., Wong, H. J., and Meiering, E. M. (2010) Energetics and mechanisms of folding and flipping the myristoyl switch in the {beta}-trefoil protein, hisactophilin. *Proc. Natl. Acad. Sci. U. S. A. 107*, 20952−20957.
(63) Bille, A., Jonsson, S. A. E., Akke, M., and Irback, A. (2013) Local unfolding and aggregation mechanisms of SOD1: a Monte Carlo exploration. *J. Phys. Chem. B 117*, 9194−9202.
(64) Ding, F., Furukawa, Y., Nukina, N., and Dokholyan, N. V. (2012) Local unfolding of Cu, Zn superoxide dismutase monomer determines the morphology of fibrillar aggregates. *J. Mol. Biol. 421*, 548−560.
(65) Hornberg, A., Logan, D. T., Marklund, S. L., and Oliveberg, M. (2007) The coupling between disulphide status, metallation and dimer interface strength in Cu/Zn superoxide dismutase. *J. Mol. Biol. 365*, 333−342.
(66) Rumfeldt, J. A., Lepock, J. R., and Meiering, E. M. (2009) Unfolding and folding kinetics of amyotrophic lateral sclerosis-associated mutant Cu,Zn superoxide dismutases. *J. Mol. Biol. 385*, 278−298.
(67) Museth, A. K., Brorsson, A. C., Lundqvist, M., Tibell, L. A., and Jonsson, B. H. (2009) The ALS-associated mutation G93A in human copper-zinc superoxide dismutase selectively destabilizes the remote metal binding region. *Biochemistry 48*, 8817−8829.
(68) Shipp, E. L., Cantini, F., Bertini, I., Valentine, J. S., and Banci, L. (2003) Dynamic properties of the G93A mutant of copper-zinc superoxide dismutase as detected by NMR spectroscopy: implications for the pathology of familial amyotrophic lateral sclerosis. *Biochemistry 42*, 1890−1899.
(69) Broom, H. R., Rumfeldt, J. A., Vassall, K. A., and Meiering, E. M. (2015) Destabilization of the dimer interface is a common consequence of diverse ALS-associated mutations in metal free SOD1. *Protein Sci. 24*, 2081.
(70) Broom, H. R. (2015) Stability and Aggregation Studies of Immature Superoxide Dismutase, In *Chemistry*; University of Waterloo, Waterloo.
(71) Khare, S. D., Caplow, M., and Dokholyan, N. V. (2006) FALS mutations in Cu, Zn superoxide dismutase destabilize the dimer and increase dimer dissociation propensity: a large-scale thermodynamic analysis. *Amyloid 13*, 226−235.
(72) Fenwick, R. B., Orellana, L., Esteban-Martin, S., Orozco, M., and Salvatella, X. (2014) Correlated motions are a fundamental property of beta-sheets. *Nat. Commun. 5*, 4070.
(73) Lindberg, M. J., Tibell, L., and Oliveberg, M. (2002) Common denominator of Cu/Zn superoxide dismutase mutants associated with amyotrophic lateral sclerosis: decreased stability of the apo state. *Proc. Natl. Acad. Sci. U. S. A. 99*, 16607−16612.
(74) Rodriguez, J. A., Shaw, B. F., Durazo, A., Sohn, S. H., Doucette, P. A., Nersissian, A. M., Faull, K. F., Eggers, D. K., Tiwari, A., Hayward, L. J., and Valentine, J. S. (2005) Destabilization of apoprotein is insufficient to explain Cu,Zn-superoxide dismutase-linked ALS pathogenesis. *Proc. Natl. Acad. Sci. U. S. A. 102*, 10516−10521.
(75) Svensson, A. K., Bilsel, O., Kayatekin, C., Adefusika, J. A., Zitzewitz, J. A., and Matthews, C. R. (2010) Metal-free ALS variants of dimeric human Cu,Zn-superoxide dismutase have enhanced populations of monomeric species. *PLoS One 5*, e10064.

DOI: 10.1021/acs.biochem.5b01133
Biochemistry 2016, 55, 1346−1361

(76) Valentine, J. S., Doucette, P. A., and Zittin Potter, S. (2005) Copper-zinc superoxide dismutase and amyotrophic lateral sclerosis. *Annu. Rev. Biochem. 74*, 563−593.
(77) Banci, L., Bertini, I., D'Amelio, N., Gaggelli, E., Libralesso, E., Matecko, I., Turano, P., and Valentine, J. S. (2005) Fully metallated S134N Cu,Zn-superoxide dismutase displays abnormal mobility and intermolecular contacts in solution. *J. Biol. Chem. 280*, 35815−35821.
(78) Banci, L., Bertini, I., D'Amelio, N., Libralesso, E., Turano, P., and Valentine, J. S. (2007) Metalation of the amyotrophic lateral sclerosis mutant glycine 37 to arginine superoxide dismutase (SOD1) apoprotein restores its structural and dynamical properties in solution to those of metalated wild-type SOD1. *Biochemistry 46*, 9953−9962.
(79) Kurobe, N., Suzuki, F., Okajima, K., and Kato, K. (1990) Sensitive enzyme immunoassay for human Cu/Zn superoxide dismutase. *Clin. Chim. Acta 187*, 11−20.
(80) Hwang, Y. M., Stathopulos, P. B., Dimmick, K., Yang, H., Badiei, H. R., Tong, M. S., Rumfeldt, J. A., Chen, P., Karanassios, V., and Meiering, E. M. (2010) Nonamyloid aggregates arising from mature copper/zinc superoxide dismutases resemble those observed in amyotrophic lateral sclerosis. *J. Biol. Chem. 285*, 41701−41711.
(81) Chattopadhyay, M., Durazo, A., Sohn, S. H., Strong, C. D., Gralla, E. B., Whitelegge, J. P., and Valentine, J. S. (2008) Initiation and elongation in fibrillation of ALS-linked superoxide dismutase. *Proc. Natl. Acad. Sci. U. S. A. 105*, 18663−18668.
(82) Lang, L., Zetterstrom, P., Brannstrom, T., Marklund, S. L., Danielsson, J., and Oliveberg, M. (2015) SOD1 aggregation in ALS mice shows simplistic test tube behavior. *Proc. Natl. Acad. Sci. U. S. A. 112*, 9878−9883.
(83) Mulligan, V. K., Kerman, A., Ho, S., and Chakrabartty, A. (2008) Denaturational stress induces formation of zinc-deficient monomers of Cu,Zn superoxide dismutase: implications for pathogenesis in amyotrophic lateral sclerosis. *J. Mol. Biol. 383*, 424−436.
(84) Kasinath, V., Sharp, K. A., and Wand, A. J. (2013) Microscopic insights into the NMR relaxation-based protein conformational entropy meter. *J. Am. Chem. Soc. 135*, 15092−15100.
(85) Namanja, A. T., Wang, X. J., Xu, B., Mercedes-Camacho, A. Y., Wilson, K. A., Etzkorn, F. A., and Peng, J. W. (2011) Stereospecific gating of functional motions in Pin1. *Proc. Natl. Acad. Sci. U. S. A. 108*, 12289−12294.
(86) Tzeng, S. R., and Kalodimos, C. G. (2012) Protein activity regulation by conformational entropy. *Nature 488*, 236−240.
(87) Magliery, T. J., Lavinder, J. J., and Sullivan, B. J. (2011) Protein stability by number: high-throughput and statistical approaches to one of protein science's most difficult problems. *Curr. Opin. Chem. Biol. 15*, 443−451.
(88) Stone, M. J. (2001) NMR relaxation studies of the role of conformational entropy in protein stability and ligand binding. *Acc. Chem. Res. 34*, 379−388.
(89) Whitley, M. J., and Lee, A. L. (2009) Frameworks for understanding long-range intra-protein communication. *Curr. Protein Pept. Sci. 10*, 116−127.
(90) Mittermaier, A., and Kay, L. E. (2004) The response of internal dynamics to hydrophobic core mutations in the SH3 domain from the Fyn tyrosine kinase. *Protein Sci. 13*, 1088−1099.
(91) Case, D. A. (2013) Chemical shifts in biomolecules. *Curr. Opin. Struct. Biol. 23*, 172−176.
(92) Wishart, D. S. (2011) Interpreting protein chemical shift data. *Prog. Nucl. Magn. Reson. Spectrosc. 58*, 62−87.
(93) Li, D. W., and Bruschweiler, R. (2012) PPM: a side-chain and backbone chemical shift predictor for the assessment of protein conformational ensembles. *J. Biomol. NMR 54*, 257−265.
(94) Robustelli, P., Stafford, K. A., and Palmer, A. G., 3rd. (2012) Interpreting protein structural dynamics from NMR chemical shifts. *J. Am. Chem. Soc. 134*, 6365−6374.
(95) van den Bedem, H., and Fraser, J. S. (2015) Integrative, dynamic structural biology at atomic resolution–it's about time. *Nat. Methods 12*, 307−318.
(96) Verma, D., Jacobs, D. J., and Livesay, D. R. (2012) Changes in Lysozyme Flexibility upon Mutation Are Frequent, Large and Long-Ranged. *PLoS Comput. Biol. 8*, e1002409.
(97) Schmidlin, T., Kennedy, B. K., and Daggett, V. (2009) Structural changes to monomeric CuZn superoxide dismutase caused by the familial amyotrophic lateral sclerosis-associated mutation A4V. *Biophys. J. 97*, 1709−1718.
(98) Schmidlin, T., Ploeger, K., Jonsson, A. L., and Daggett, V. (2013) Early steps in thermal unfolding of superoxide dismutase 1 are similar to the conformational changes associated with the ALS-associated A4V mutation. *Protein Eng., Des. Sel. 26*, 503−513.
(99) Taylor, J. R. (1982) *An Introduction to Error Analysis*; University Science Books, Mill Valley, CA.
(100) Vassall, K. A., Stubbs, H. R., Primmer, H. A., Tong, M. S., Sullivan, S. M., Sobering, R., Srinivasan, S., Briere, L. A., Dunn, S. D., Colon, W., and Meiering, E. M. (2011) Decreased stability and increased formation of soluble aggregates by immature superoxide dismutase do not account for disease severity in ALS. *Proc. Natl. Acad. Sci. U. S. A. 108*, 2210−2215.
(101) Koradi, R., Billeter, M., and Wuthrich, K. (1996) MOLMOL: a program for display and analysis of macromolecular structures. *J. Mol. Graphics 14* (1), 51−55.
(102) Mulder, F. A., Mittermaier, A., Hon, B., Dahlquist, F. W., and Kay, L. E. (2001) Studying excited states of proteins by NMR spectroscopy. *Nat. Struct. Biol. 8*, 932−935.

DOI: 10.1021/acs.biochem.5b01133
Biochemistry 2016, 55, 1346−1361